Disrupting LXRα phosphorylation promotes FoxM1 expression and modulates atherosclerosis by inducing macrophage proliferation

Short title: LXRα phosphorylation modulates atherosclerosis

Gage M. C.[1], Bécares N.[1], Louie R.[1], Waddington K.[1], Zhang Y.[1], Tittanegro T.H.[1], Rodríguez-Lorenzo S.[2], Jathanna A.[1], Pourcet B.[1#], Pello O.[1§], De la Rosa J.V.[2], Castrillo A.[2] and Pineda-Torra I.[1]

[1]Centre for Clinical Pharmacology, Division of Medicine, University College of London, 5 University Street, London, WC1 E6JF, United Kingdom.

[2] Instituto de Investigaciones Biomédicas "Alberto Sols" CSIC-Universidad Autónoma de Madrid, Spain, Unidad de Biomedicina (Unidad Asociada al CSIC), Instituto Universitario de Investigaciones Biomédicas y Sanitarias (IUIBS), Grupo de Investigacion Medio Ambiente y Salud (GIMAS, ULPGC). Universidad de Las Palmas de Gran Canaria, Las Palmas, Spain.

Corresponding author:
Inés Pineda-Torra, E-mail: i.torra@ucl.ac.uk

New address: European Genomic Institute for Diabetes (EGID), FR 3508, University of Lille, INSERM UMR 1011, CHU Lille; Institut Pasteur de Lille, F-59000 Lille, France.

§ New address: The John Goldman Center for Cellular Therapy, Hammersmith Hospital, Imperial College Healthcare NHS Trust, W12 0HS London.

ABSTRACT

Macrophages are key immune cells for the initiation and development of atherosclerotic lesions. However, the macrophage regulatory nodes that determine how lesions progress in response to dietary challenges are not fully understood. Liver X receptors (LXRs) are sterol-regulated transcription factors which play a central role in atherosclerosis by integrating cholesterol homeostasis and immunity. LXR pharmacological activation elicits a robust anti-atherosclerotic transcriptional program in macrophages that can be affected by LXRα S196 phosphorylation *in vitro*. To investigate the impact of these transcriptional changes in atherosclerosis development, we have generated mice carrying a Ser-to-Ala mutation in myeloid cells in the LDLR-deficient atherosclerotic background (M-S196A$^{Ldlr\text{-}KO}$). M-S196A$^{Ldlr\text{-}KO}$ mice fed a high fat diet exhibit increased atherosclerotic plaque burden and lesions with smaller necrotic cores and thinner fibrous caps. These diet-induced phenotypic changes are consistent with a reprogramed macrophage transcriptome promoted by LXRα-S196A during atherosclerosis development. Remarkably, expression of several proliferation-promoting factors including the proto-oncogene FoxM1 and its targets are induced by LXRα-S196A. This is consistent with increased proliferation of plaque-resident cells in M-S196A$^{Ldlr\text{-}KO}$ mice. Moreover, disrupted LXRα phosphorylation increases expression of phagocytic molecules resulting in increased apoptotic cell removal by macrophages, explaining the reduced necrotic cores. Finally, the macrophage transcriptome promoted by LXRα-S196A under dietary perturbation is markedly distinct from that revealed by LXR ligand activation, highlighting the singularity of this post-translational modification. Overall, our findings demonstrate that LXRα phosphorylation at S196 is an important determinant of atherosclerotic plaque development through selective changes in gene transcription that affect multiple pathways.

SIGNIFICANCE

To date, LXR importance in atherosclerosis development has been gleaned from their pharmacological or genetic manipulation. Here we show that altering LXRα phosphorylation can shape pro-atherogenic responses to fat-rich diets, uncovering previously unrecognized mechanisms. Disrupting LXRα phosphorylation in myeloid cells triggers global changes in gene expression in macrophages including the up-regulation of proliferation-promoting factors, consistent with increased proliferation of lesion-resident cells. This leads to an enhanced atherosclerotic plaque burden and plaques with altered phenotypic features. Notably, novel LXRα-regulated targets revealed by impaired LXRα phosphorylation are markedly distinct from those promoted by LXR ligand activation. Overall, this work reveals LXRα phosphorylation as an

important determinant of atherosclerosis development. This could be exploited for the design of novel anti-atherosclerotic strategies.

\body

INTRODUCTION

Atherosclerosis is a chronic inflammatory process and the major pathology responsible for cardiovascular disease, which is now the leading cause of global mortality(1). This pathology results from the accumulation of lipids, immune cells and extracellular matrix within arterial walls, causing flow limitation(2). Atherosclerotic lesions progress and may rupture and thrombose, occluding the vessel and leading to myocardial infarcts or strokes. Macrophages are immune cells involved in most key pathways for the development of atherosclerosis including uptake of oxidized LDL, cholesterol efflux, foam cell and fatty streak formation, local proliferation, apoptosis, programmed removal of dead cells or efferocytosis, necrotic core formation and contribution to plaque stability(2).

Liver X receptors (LXRs) are ligand activated transcription factors that play vital roles in cholesterol homeostasis(3) and inflammation(4). LXRs are expressed as two isotypes; LXRα and LXRβ, which display 78% sequence homology, yet vary in their tissue expression and regulation(5). Both LXRs are endogenously activated by oxidized metabolites of cholesterol(6) and intermediates of the cholesterol biosynthesis pathway(7), as well as by various synthetic ligands(8). Pharmacological activation of these receptors has been demonstrated to modulate a range of lipid and inflammatory disorders(9). With regards to atherosclerosis, activating LXRs attenuates atherosclerosis progression(3) via promotion of cholesterol efflux through lipid-laden macrophages present in the atherosclerotic lesions, inhibition of vascular inflammation(4) and possibly by affecting other aspects of lipid metabolism(10). Additionally, ligand-activated LXR promotes CCR7-dependent plaque regression(11). Functional studies in macrophages further indicate that LXRα is required for a robust anti-atherosclerotic response to LXR ligands and LXRα plays a selective role in limiting atherosclerosis in response to hyperlipidemia(12).

LXRα transcriptional activity can be modulated by several posttranslational modifications(5) including phosphorylation at serine (S) 198 in the human sequence, corresponding to S196 in the mouse orthologue. We have demonstrated that modulation of LXRα phosphorylation significantly modifies its target gene repertoire in macrophage cell lines overexpressing the receptor, thereby altering pathways known to be relevant to the development of atherosclerosis(13, 14). Interestingly, we previously showed phosphorylated S196-LXRα is present in progressive atherosclerotic lesions(14) suggesting LXRα phosphorylation at this residue could be important for the development of atherosclerotic plaques. However, the specific contribution of myeloid LXRα phosphorylation to atherosclerosis development remains unknown.

To investigate this, we have generated a mouse model specifically expressing a Ser-to-Ala phosphorylation mutant of LXRα in myeloid cells (M-S196A) in the LDLR-deficient (Ldlr-KO) atherosclerotic background (M-S196A$^{Ldlr\text{-}KO}$). Disrupting LXRα phosphorylation in myeloid cells including macrophages promotes plaque burden, yet modulates plaque phenotype to acquire distinctive characteristics such as smaller necrotic cores and thinner fibrous caps encapsulating the lesions. These phenotypic changes are consistent with a reprogrammed macrophage transcriptome. Notably, cell cycle progression and proliferation pathways are markedly induced in M-S196A$^{Ldlr\text{-}KO}$ macrophages, specifically the expression of the FoxM1 transcription factor and several of its targets. This is associated with increased lesion-resident cell proliferation in the LXRα phospho-mutant mice. In addition, changes in the expression of various phagocytic molecules result in enhanced macrophage efferocytosis thus explaining the reduced necrotic cores present in M-S196A mice. Interestingly, most of the phosphorylation sensitive genes identified are not subject to LXR ligand regulation and we show that global transcriptional changes in response to impaired LXRα phosphorylation under dietary perturbation are markedly distinct from those revealed by ligand activation. Overall, these findings demonstrate LXRα phosphorylation at S196 determines atherosclerotic plaque progression by promoting changes in local cell proliferation, efferocytosis and necrotic core formation.

RESULTS

Impaired myeloid LXRα phosphorylation promotes atherosclerosis

To investigate the impact of macrophage LXRα phosphorylation on the development of atherosclerosis we generated a new mouse model expressing a serine to alanine mutation at residue 196 in LXRα in myeloid cells (M-S196A) on a pro-atherosclerotic (LDLR-deficient or Ldlr-KO) background (M-S196A$^{Ldlr\text{-}KO}$) (Fig. S1A). Effective expression of Cre-driven targeting construct introducing S196A knock-in in the sense strand was demonstrated in M-S196A$^{Ldlr\text{-}KO}$ compared to WT$^{Ldrl\text{-}KO}$ control littermates (Fig. S1B). Mice were fed a fat-rich Western diet (WD) to accelerate plaque progression. LXRα expression was similar in WT$^{Ldlr\text{-}KO}$ and M-S196A$^{Ldlr\text{-}KO}$ mice (Fig. S1C,D). M-S196A$^{Ldlr\text{-}KO}$ mice developed normally and no change in body weight before, during or after Western diet (WD) feeding was observed (Fig. S1E-G). There were no detectable changes in basal metabolic characteristics including total cholesterol, HDL or LDL/VLDL levels and amount of triglycerides, free fatty acids and insulin in the plasma of M-S196A$^{Ldlr\text{-}KO}$ compared to WT$^{Ldlr\text{-}KO}$ (Fig. S2A-G). Interestingly, M-S196A$^{Ldlr\text{-}KO}$ mice showed a significant increase in atherosclerosis plaque burden in their aortas as measured by *en face* oil red O staining (Fig. 1A) and aortic root plaque coverage (Fig. 1B,C). This was however, not associated with changes in the levels of CD68+ positive cells in the lesions (Fig. 1D).

Changes in LXRα phosphorylation at Ser196 reprogram global macrophage gene expression in the context of diet-induced atherosclerosis

To explore in more detail the pathways underlying the changes observed in atherosclerosis development we investigated the transcriptomic profiles of macrophages differentiated from the bone marrows of mice exposed to the WD. RNA-seq analysis revealed significant genome wide changes in transcript levels (Fig. 2A,B). LXRα-S196A significantly induced (460) or reduced (210) gene expression. The impact of LXRα-S196A on the basal macrophage expression of well-established LXR targets varied: while *Srebf1* and *Abcg1* levels were not affected, other targets such as *Abca1* and *Apoe* were significantly reduced (Fig. S3A). Hallmark pathway analysis identified G2/M checkpoint and E2F targets to be markedly enriched indicating cell cycle and cell proliferation pathways are induced in the mutant-expressing macrophages (Fig 2C and Fig. S4A,B). This was further confirmed by Reactome pathway analysis (Table S1). Several genes involved in these processes were regulated over 2-fold including cell proliferation marker *Mik67* or Ki67 (4.58-fold, p=3.46E-43) (Fig 2D). Concomitant to these changes in cell proliferation genes, there was a substantial reduction in the expression of genes associated with the immune response (Fig 2C,E, Fig. S4C and Table S2). We observed opposing changes in the expression of chemokine receptors involved in monocyte trafficking to atherosclerotic lesions and some of the chemokines they bind to(15) (Fig. 2F). For example, expression of the chemokine receptors *Ccr1* (1.43-fold, P=0.004), *Ccr2* (1.73-fold, P=3.8x10^{-15}) and *Cx3cr1* (1.8-fold, P=0.0008) was increased whereas *Ccr5* (0.55-fold, P=6.19x10^{-17}) expression was diminished in LXRα-S196A macrophages compared to WT macrophages. Such differential expression of chemokine receptors and their ligands may explain the lack of change in the overall number of CD68+ cells retained in the plaques of M-S196A$^{Ldlr\text{-}KO}$ mice. Furthermore, there was no difference in the number of circulating monocytes between genotypes (Fig. S1H).

M-S196A induces expression of FoxM1 and lesion-resident cell

Examination of the RNA-seq datasets revealed LXRα-S196A cells expressed almost 3-fold (p=7.76E-14) more proto-oncogene FoxM1 compared to macrophages expressing wild type LXRα (Fig. 3A, Fig. S3D). This was also the case for several FoxM1 target genes(16) (Fig. 3A, Fig. S3D). While LXRα activation was previously shown to inhibit cell proliferation via inhibition of FoxM1 in hepatic carcinoma cells(17), its regulation in macrophages has never been documented. LXRs modulate gene transcription by heterodimerising with the Retinoid X Receptor (RXR) and binding to specific DNA sequences termed LXR response elements (LXREs) in the transcriptional regulatory regions of their target genes(18). Similar to the well-known *Srebf1* LXR target (Fig. 3B), specific LXRα occupancy was observed at the *FoxM1* gene in macrophages at different sites (Fig. 3D) further indicating that *FoxM1* is an LXRα target in these cells. These sites were initially

identified by ChIPseq analysis (Fig. S5A) and *in silico* by sequence similarity to reported LXREs. We also confirmed that, unlike *FoxM1*, genes upstream of this gene were not significantly influenced by the expression of LXRα-S196A in macrophages (Fig. S5B). Contrary to *Srebf1*, which is not affected by LXRα-S196A expression, LXRα occupancy as well as H3K27 acetylation at *FoxM1* and at one of its targets, *Cenpf*, were modestly enhanced in macrophages expressing the phospho-mutant receptor, suggesting this may be one of the mechanisms by which LXRα-S196A influences the expression of these genes. The enhanced levels of several pro-mitotic genes suggested cell proliferation could be altered in M-S196A$^{Ldlr\text{-}KO}$ macrophages. Indeed, macrophages expressing the LXRα-S196A mutant showed about 20% increase in proliferation in culture measured as Ki67 levels (Fig. S5C,D). Recent studies have highlighted the important role local macrophage proliferation plays in lesion development(19). Consistent with a significant increase in the regulation of *FoxM1* and other genes involved in cell cycle pathways, increased proliferation of lesion-resident cells as measured by Ki67 staining was observed in the atherosclerotic plaques of M-S196A$^{Ldlr\text{-}KO}$ mice (Fig. 3B) which was associated with increased nuclei content (Fig. S6B) compared to WT$^{Ldlr\text{-}KO}$. Notably, pharmacological inhibition of FoxM1 using the specific inhibitor FDI-6(20, 21), reduced the enhanced M-S196A$^{Ldlr\text{-}KO}$ macrophage proliferation observed (Fig. 3G, H) and consistently reduced FoxM1 target gene expression (Fig. 3I), confirming that FoxM1 upregulation mediates, at least in part, some of the increased macrophage proliferation observed in M-S196A$^{Ldlr\text{-}KO}$ mice. This strongly suggests that FoxM1-dependent enhanced local proliferation in the plaques could contribute to increased plaque size exhibited by M-S196A$^{Ldlr\text{-}KO}$ mice as has been postulated(22–24).

M-196A$^{Ldlr\text{-}KO}$ mice display phenotypic changes in their necrotic cores and fibrous caps

The observed changes in gene expression suggest a complex interaction of pathways involved in the progression of atherosclerosis. Unexpectedly, despite their larger size, size-matched atherosclerotic lesions in M-S196A$^{Ldlr\text{-}KO}$ mice display smaller necrotic cores (Fig. 4A). Programmed cell removal or efferocytosis has been shown to strongly impact the formation of necrotic cores in advanced plaques(25). In agreement with this, macrophage engulfment of apoptotic cells was significantly increased (Fig. 4B and Fig. S6C). Further interrogation of the LXRαS196A-regulated transcriptome showed differential expression of several pro- and anti-phagocytic molecules (Fig. 4C and Fig. S3B). This includes *Ccr2* (1.73-fold, P=3.8x10^{-15}), *Gpr132* (1.64-fold, P=1.73x10^{-10}), Itgb3 (1.59-fold, P=0.007) and *Mfge8* (1.37-fold, P=7.46x10^{-5}) known to promote efferocytosis(25) as well as molecules known to render apoptotic cells resistant to efferocytosis such as *Cd47*(26) (0.75-fold, P=0.0001) and *Tnf* (0.71-fold, P=0.0004) in M-S196A$^{Ldlr\text{-}KO}$ macrophages. This is consistent with the enhanced efferocytosis observed in these cells. Another important morphological feature of atherosclerotic lesions influenced by

macrophages is the thinning of the protective collagenous scar surrounding it or fibrous cap(27). Interestingly, M-S196A$^{Ldlr\text{-}KO}$ lesions show reduced fibrous cap thickness with overall smaller fibrous cap areas (Fig. S6D,E). This could result from the diminished expression of several collagen genes including *Col1a1* (0.6-fold, P=9.3x10^{-04}), *Col1a2* (0.7-fold, P=9.9x10^{-03}), *Col3a1* (0.6-fold, P=4.0x10^{-03}), *Col5a1* (0.6-fold, P=3.4x10^{-03}), and *Col6a1* (0.5-fold, P=4.2x10^{-05}) and increased levels of matrix degrading molecules such as *Mmp8* (1.57-fold, P=6.1x10^{-10}) and *Mmp12* (1.48-fold, P=8.8x10^{-6}). Overall, this data highlights the complex phenotypic changes present in atherosclerotic lesions resulting from changes in LXRα phosphorylation.

Disrupted LXR*α *phosphorylation at Ser196 alters ligand responses in macrophages.

Our findings indicate that in the context of an atherogenic diet, changes in LXRα phosphorylation modulate the macrophage transcriptome and promote atherosclerotic plaque burden. To further understand the magnitude of the transcriptional changes imposed by the LXRα phosphorylation mutant, we next examined whether WT and S196A expressing macrophages respond differently to an LXR ligand and explored the differences in global transcript changes between ligand activation and reduced LXRα phosphorylation. RNA-seq analysis was performed on bone marrow-derived macrophages from M-196A$^{Ldlr\text{-}KO}$ mice exposed to WD for 12 weeks and cultured in the presence of vehicle or LXR ligand GW3965. GW ligand activation promoted changes in macrophage gene expression that were different in cells expressing the S196A mutant compared to WT macrophages (Fig. S7A,B,C). GSEA analysis revealed the pathways subject to changes in LXRα phosphorylation in the presence of the LXR ligand are similar to those seen in the absence of GW (Fig. S7D). For instance, genes involved in nuclear division and cell cycle regulation remained strongly induced by LXRα-S196A, further emphasizing the importance of LXRα phosphorylation in the modulation of these pathways. Remarkably, it became apparent that while a small subset of genes were differentially regulated by the mutant only in the context of the ligand (94 induced and 50 reduced compared to WT cells), most differences in gene expression were observed in the absence of ligand (Fig. 5A,B). Additionally, our datasets also showed that ligand responses (either induction or repression) were similar in both WT and mutant expressing macrophages for a subset of genes but not for others (Fig. 5C and Fig. S8A-D). Further analysis revealed that both the magnitude of the response and the identity of the genes were strikingly different between the response to the ligand (regulation by GW in either WT or S196A cells) and to phosphorylation (modulation by LXRα-S196A compared to WT) (Fig. S7E,F). This highlights the significance of S196 phosphorylation in rewiring the LXR-modulated transcriptome.

Finally, we investigated whether this dichotomy between ligand and phosphorylation-induced responses was apparent in the regulation of the phosphorylation-sensitive gene *FoxM1* and some

of its target genes. *FoxM1* was not significantly affected by exposure to the LXR ligand in WT^{LdlrKO} cells (Fig. 5D,E). By contrast, GW3965 activation markedly reduced *FoxM1* mRNA levels in M-S196A$^{Ldlr\text{-}KO}$ macrophages (Fig. 5D,E). This regulatory pattern was recapitulated by most *FoxM1* targets examined. In addition, established transcriptional regulators of *FoxM1* were strongly (*Top2a, Rad51, Check2*) or moderately (*Melk*) induced in M-S196A$^{Ldlr\text{-}KO}$ cells in unstimulated conditions compared to WT^{LdlrKO} cells (Fig. 5F). Consistent with the known anti-proliferative effects of LXR ligands, the expression of these genes was strongly attenuated by GW3965, although this occurred preferentially in the mutant cells. Other LXRα phosphorylation-sensitive genes implicated in cell cycle progression mimic this mode of regulation (Fig. S7G).

Overall, our findings suggest that LXRα phosphorylation at Ser196 is a powerful means of regulating LXRα transcriptional activity that has important consequences for macrophage biology and for the progression of a metabolic, inflammatory and proliferative disease such as atherosclerosis.

DISCUSSION

The macrophage regulatory nodes that determine how the atherosclerotic lesion progresses in response to dietary challenges are not fully understood. Liver X receptors have key roles in the regulation of macrophage lipid homeostasis and inflammation and as such they strongly modulate the progression of metabolic diseases such as atherosclerosis(3). The importance of these receptors in disease development has been mainly gleaned from studies evaluating the consequences of its pharmacological or genetic manipulation. However, it remained unknown whether alternative modulation of the activity of these receptors, for instance, by altering post-translational modifications of the receptor, could shape the pro-atherogenic responses of fat-rich diets thus altering disease development. We previously showed LXRα is phosphorylated in cholesterol-loaded macrophages and in progressive atherosclerotic plaques(13). We have now explored the impact of LXRα phosphorylation on atherosclerosis development by expressing an LXRα Ser196-to-Ala mutant, previously shown to disrupt LXRα phosphorylation(13), specifically in myeloid cells on the LDLR null background (M-LXRαS196A$^{Ldlr\text{-}KO}$).

LXRαS196A expression in cells of the myeloid lineage, including macrophages, increases atherosclerotic plaque burden (Fig. 1 and Fig.S9). This is consistent with an enhanced number of proliferating lesion-resident cells (Fig. 3E) in M-LXRαS196A$^{Ldlr\text{-}KO}$ mice and the up-regulation of genes driving cell cycle progression in macrophages, particularly at the G2/M checkpoint, accounting for up to 15% of the total changes in gene expression exerted by the phosphorylation mutant (Fig. 2C). During the past decade established paradigms of atherosclerotic plaque

formation and progression have been revisited and local proliferation of macrophages has been demonstrated to be an important driver of atherosclerosis development in advanced atherosclerotic plaques(22, 24, 28). However, the specific players modulating macrophage proliferation in the context of atherosclerosis remain poorly understood. Proliferation of lesional macrophages has been linked to up-regulation of the scavenger receptor Msr1(22, 29) but a defined mechanism has remained elusive. Our findings now indicate that modulation of LXRα phosphorylation plays an important role in this process.

LXRs are known modulators of cell proliferation in other disease conditions where cell proliferation is critical, including cancer(30). For instance, LXR activation inhibits proliferation of B and T cells and macrophages(31–33) and several cancer cell lines including prostate (LNCaP)(34), breast (MCF7)(35) and colon (HTC111)(36). Identified anti-proliferative mechanisms by classic LXR agonists appear to be independent of the lipogenic activity of LXR(35), but rather linked to βcatenin activity(36), cyclins(34) and sterol metabolism(33). In contrast to these inhibitory effects, LXR activation was recently reported to enhance proliferation of neural progenitor cells in a MEK-ERK pathway dependent manner(37). Inverse agonism of LXR with a novel synthetic agonist has also shown promise as a potential cancer treatment though inhibition of lipogenesis, glycolysis and by regulating the expression of key glycolytic and lipogenic genes(30). However this is the first time LXR is shown to target cell cycle promoting factors in an atherosclerotic context.

The underlying mechanisms explaining the reported LXR anti-proliferative actions may be cell-specific. The inhibitory effects of LXR ligands on M-CSF-stimulated macrophage proliferation involve the down-regulation of the cyclin dependent kinase regulators cyclin D1 (*Ccnd1*) and B1 (*Ccnb1*)(32). Both cyclins are inhibited by LXRα through the transcriptional repression of FoxM1 in hepatic carcinoma cells(17). Conversely, LXR antagonism with a sulphated oxysterol promotes hepatic proliferation in part through the induction of FoxM1(38). FoxM1 is an essential proliferation-associated transcription factor found overexpressed in numerous solid tumors(39–42). Its expression is restricted to actively dividing cells, and is regulated in a cell-cycle dependent manner by a wide range of proliferative signals(43). FoxM1 levels are induced in the G1-phase, maintained throughout the S- phase and reaching maximum expression in the G2/M-phase(44–47). We now demonstrate that chronic disruption of LXRα phosphorylation in macrophages enhances FoxM1 expression and several of its associated regulators and targets driving cell cycle progression(16) (Fig. 3A, Fig. S3D). We have now identified multiple LXRα binding sites at the FoxM1 locus, confirming *FoxM1* is a novel LXR target in macrophages (Fig. 3C). LXRα occupancy and H3K27 acetylation is modestly enhanced at some of these sites in cells expressing the LXRα phospho-mutant, indicating this is likely one of the mechanisms underlying enhaced *FoxM1*

expression in these cells. It is possible that expression of the S to A mutant could affect the structure/function of LXRα unrelated to its impact on the phosphorylation of the receptor. Nevertheless, we have previously shown by molecular modelling that phosphorylated and non-phosphorylated receptor can adopt different structures that could influence protein-protein interactions ultimately modulating LXRα function(14). Importantly, induced *FoxM1* levels are associated with increased lesional cell proliferation (Fig. 3E) and cell content (Fig. S6B), consistent with larger atherosclerotic lesions. Amongst FoxM1 regulators, Bub1b (or BubR1, increased 1.9 fold, $P=1.26x10^{-6}$ in the LXRα-S196A-expressing macrophages) has been shown to alter atherosclerosis, as impaired expression of BubR1 results in decreased macrophage proliferation and attenuated atherogenesis(48). Furthermore, LXRα-S196A macrophages show decreased mRNA expression of the FoxM1 inhibitor SASH1(49) (0.8-fold, $P=1.33x10^{-4}$), which was implicated in the development of atherosclerosis in people that smoke through its monocytic monocyte up-regulation. Notably, we now provide evidence that specific inhibition of FoxM1 reduces proliferation of LXRα-S196A macrophages, confirming the relevance of this pathway. Overall, our findings further highlight the importance of this set of molecules in atherosclerosis progression.

Importantly, we show evidence that reduced LXRα phosphorylation during atherosclerosis development reprograms the macrophage transcriptome (Fig. 2). Global gene expression analysis revealed that in these cells, most genes are sensitive to the expression of the LXRα phosphomutant in the absence of LXR ligand stimulation, with only an additional 82 genes being modulated by the mutant in the presence of the GW3965 ligand compared to the 670 LXRα phosphorylation sensitive genes under basal conditions (Fig. S7E,F). This suggests that modulation by LXRα-S196A expression is different from the regulation by ligand activation of the receptor. Indeed, comparison of the various datasets evidenced that the transcriptomic rewiring in response to impaired LXRα phosphorylation in the mutant cells is remarkably distinct and does not merely phenocopy ligand responses (Fig. 5C and Fig. S8C,D) thus highlighting the importance of this post-translational modification in modulating the activity of LXRα in the context of a metabolic and inflammatory disease. An example for this, is the regulation of *FoxM1* expression and its regulated pathways, which are induced in LXRα-S196A-expressing cells (Fig. 3A and Fig. S3D). Previous reports have linked LXRα activation with *FoxM1* repression in hepatic carcinoma cells(17). We observed that FoxM1 inhibition by GW3965 is recapitulated in macrophages from mice exposed to a high fat diet that are developing atherosclerotic plaques (Fig. 5D,E). However, this is preferentially observed in the LXRα phosphorylation mutant-expressing cells. In fact, most FoxM1 targets and modulators as well as other factors involved in the G2/M cell cycle transition mirror this pattern of regulation (Fig. 5E,F and Fig. S7G). This suggests that in macrophages, the

anti-proliferative effects of LXR ligands are enhanced when LXRα phosphorylation is disrupted. Intriguingly, these transcriptomic changes are observed in cells that have been differentiated and cultured *in vitro* from precursor cells exposed to the pro-atherosclerotic environment in the bone marrow of WD-fed mice and could be the result of epigenetic changes influenced by the diet. Indeed, there are reports showing a distinct metabolic environment (for instance in type 2 diabetes) can epigenetically imprint bone marrow progenitor cells that can derive into a "pre-programmed" macrophage state associated with changes in gene expression(50). Outside the scope of this study, future investigations will help establish changes in the epigenome of LXRα-S196A expressing cells and how they affect metabolic, proliferative and inflammatory pathways..

The observed changes in gene expression are likely to result from a combination of factors, including differential binding to DNA (as shown in Fig. 3D) and possibly variations in the interaction with cofactors. Indeed, we have previously described that differential NCoR binding to the LXR phospho-mutant is important for the variation in the expression of certain targets (13). In addition, we have shown using molecular modelling, how LXRα in its unphosphorylated state may impact cofactor interactions by exposing an alternative surface for protein interaction(14). Thus, a mutation disrupting phosphorylation would be expected to mimic these interactions *in vivo*, which could also partly explain the observed changes in gene expression. Based on this molecular modelling, it is currently unclear how the change in LXR phosphorylation at this serine residue could impact DNA binding. The S198 residue does not contact directly with DNA or the RXRalpha DNA binding domain. However, this was examined for one particular LXRE and may likely vary at different LXREs/DNA sequences, thus explaining the gene gene-specific effects observed when the phospho-mutant is expressed. Future investigations beyond the scope of this study comparing global WT and phospho-mutant LXR DNA binding profiles will be able to provide further insight into the molecular mechanisms behind the observed differences in gene expression.

Beyond changes in cell proliferation, the enhanced plaque burden in M-LXRαS196A$^{Ldlr\text{-}KO}$ mice is likely the result of the complex modulation of additional pathways relevant for atherosclerosis development. LXRα promotes the expression of factors important for macrophage efferocytotic capacity such as the MerTK receptor for apoptotic cells(51) which can influence the formation of the necrotic core and plaque stability(52). Despite the overall increase in atherosclerosis, we found that size-matched advanced plaques from M-S196A$^{Ldlr\text{-}KO}$ mice exhibited significantly reduced necrotic cores (Fig. 4A) consistent with the increased capacity of M-S196A$^{Ldlr\text{-}KO}$ macrophages to engulf apoptotic cells (Fig. 4B and Fig. S6C). Transcriptomic profiling revealed that in addition to the reduced expression of Mertk and its ligand Gas6, several genes known to promote phagocytosis were significantly upregulated in M-S196A$^{Ldlr\text{-}KO}$ cells, including the pro-phagocytotic receptors Ccr2(53), Gpr132(54), Itgb3(55) and the bridging molecule

Mfge8(56) (Fig. 4C and Fig. S3B). This differential expression could explain the increased phagocytic ability of the LXRα phospho-mutant expressing macrophages (Fig. 4B).

With regards to the signals that may regulate LXRα phosphorylation in the context of atherosclerosis progression, we previously showed that LXRα is phosphorylated at this same residue both in response to cholesterol loading in cultured macrophages and in foam cells within atherosclerotic plaques from animal models fed a high fat diet(13). A possible candidate could be desmosterol (a cholesterol precursor and the last intermediate in the Bloch biosynthesis pathway), that accumulates in macrophage foam cells and atherosclerotic plaques(7) and acts as an endogenous LXR ligand modulating its target gene expression(7, 57). Desmosterol promotes phosphorylation of LXRα in macrophages in culture (Fig. S10) and could be one of the many signals that affects LXRα phosphorylation in an atherosclerotic environment, although it is likely that a combination of them is responsible for ultimately promoting this modification**.** It is possible that endogenous cues preventing LXRα phosphorylation, thus mimicking the Ser to Ala mutation, may alter cell proliferation and phagocytosis in a similar manner. However, they are also likely to exert other (similar or opposing) effects to other transcription factors or signalling molecules. Future studies will aim to further identify endogenous signals modulating LXRα phosphorylation in the context of atherosclerosis.

In summary, we have shown that disrupting LXRα phosphorylation in cells of the myeloid lineage, affects the development of atherosclerosis that could be explained through altered cell proliferation and efferocytosis. We also show that chronically modulating LXRα phosphorylation reprograms gene regulation in macrophages under basal conditions and significantly affects their response to ligand stimulation. These findings add to our fundamental knowledge of how LXRα activity can be regulated and introduce novel functional consequences of its modification by phosphorylation which should be heeded to manipulate these receptors for the design of novel cardiovascular therapies.

MATERIALS AND METHODS

Analysis of Murine Atherosclerosis Development. $WT^{Ldlr\text{-}KO}$ and $M\text{-}S196A^{Ldlr\text{-}KO}$ mice were generated as described in *SI Materials and Methods*. All procedures were carried under the UK's Home Office Animals (Scientific Procedures) Act 1986. Eight-week old $WT^{Ldlr\text{-}KO}$ and $M\text{-}S196A^{Ldlr\text{-}KO}$ male mice were fed ad libitum a Western diet (WD) (20% Fat, 0.15% Cholesterol; #5342 AIN-7A, Test Diet Limited, UK) for 12 weeks. Murine atherosclerosis and lesion characterisation was performed as described in *SI Materials and Methods.*

Cell Culture and in vitro experiments. Bone marrow derived macrophage culture. Bone Marrow-derived Macrophages (BMDM) were prepared as in(58). Peritoneal macrophages and Jurkat cells were prepared as described in *SI Materials and Methods.* Efferocytosis assay and flow cytometry was performed as described in *SI Materials and Methods.*

Gene expression analysis. RNA quantification, RT-qPCR, RNA sequencing and analysis were performed as described in *SI Materials and Methods.*

AUTHOR CONTRIBUTIONS

M.G. performed most experiments, data analysis and prepared figures. N.B. performed experiments and helped with RNAseq analysis. K.W., T.T. and A.J. performed qPCR and analysed data. R.L performed ChIP qPCR experiments. K.W. performed proliferation and monocytosis analysis. B.P. and O.M.P. helped establish mouse colonies. J.V.R and A.C. performed ChIPseq analysis. Z.Y. performed efferocytosis assays. M.G. and I.P.T designed experiments, analysed and interpreted data and wrote the manuscript. I.P.T. conceived the study, secured funding and supervised all aspects of the work.

ACKNOWLEDGEMENTS

We are grateful to Prof Edward Fisher and Prof Michael Garabedian (NYU School of Medicine) for their insightful discussions and Theresa Leon for providing Jurkat cells. This work was supported by a Medical Research Council New Investigator Grant G0801278 (IPT), British Heart Foundation Project Grant PG/13/10/30000 (IPT), UCL Grand Challenges PhD Studentship (IPT), BHF Studentship FS/12/59/30649 (IPT), and the Royal Free Charity PhD Program in Medicine (IPT), and SPANISH MINECO grants SAF2014-56819-R (AC), SAF2015-71878-REDT (AC). T.T was funded by São Paulo Research Foundation (FAPESP) grant#2017/12314-0.

REFERENCES

1. Roth GA, et al. (2015) Global and regional patterns in cardiovascular mortality from 1990 to 2013. *Circulation* 132(17):1667–78.
2. Moore KJ, Sheedy FJ, Fisher E a (2013) Macrophages in atherosclerosis: a dynamic balance. *Nat Rev Immunol* 13(10):709–21.
3. Lee SD, Tontonoz P (2015) Liver X receptors at the intersection of lipid metabolism and atherogenesis. *Atherosclerosis* 242(1):29–36.
4. Pascual-García M, Valledor AF (2012) Biological Roles of Liver X Receptors in Immune Cells. *Arch Immunol Ther Exp (Warsz)* 60(4):235–249.
5. Becares N, Gage MC, Pineda-Torra I (2017) Posttranslational Modifications of Lipid-

Activated Nuclear Receptors: Focus on Metabolism. *Endocrinology* 158(2):213–225.
6. Janowski BA, Willy PJ, Devi TR, Falck JR, Mangelsdorf DJ (1996) An oxysterol signalling pathway mediated by the nuclear receptor LXRα. *Nature* 383(6602):728–731.
7. Spann NJ, et al. (2012) Regulated accumulation of desmosterol integrates macrophage lipid metabolism and inflammatory responses. *Cell* 151(1):138–52.
8. Collins JL, et al. (2002) Identification of a nonsteroidal liver X receptor agonist through parallel array synthesis of tertiary amines. *J Med Chem* 45(10):1963–1966.
9. Hong C, Tontonoz P (2014) Liver X receptors in lipid metabolism: opportunities for drug discovery. *Nat Rev Drug Discov* 13(6):433–444.
10. Ito A, et al. (2015) LXRs link metabolism to inflammation through Abca1-dependent regulation of membrane composition and TLR signaling. *Elife* 4:e08009.
11. Feig JE, et al. (2010) LXR promotes the maximal egress of monocyte-derived cells from mouse aortic plaques during atherosclerosis regression. *J Clin Invest* 120(12):4415–4424.
12. Bischoff ED, et al. (2010) Non-redundant roles for LXR and LXR in atherosclerosis susceptibility in low density lipoprotein receptor knockout mice. *J Lipid Res* 51(5):900–906.
13. Torra IP, et al. (2008) Phosphorylation of liver X receptor alpha selectively regulates target gene expression in macrophages. *Mol Cell Biol* 28(8):2626–36.
14. Wu C, et al. (2015) Modulation of macrophage gene expression via LXRα serine 198 phosphorylation. *Mol Cell Biol* 35(11):2024–2034.
15. Ley K, Pramod AB, Croft M, Ravichandran KS, Ting JP (2016) How Mouse Macrophages Sense What Is Going On. *Front Immunol* 7:204.
16. Nag A, Chakraborty S Biology of FOXM1 and its Emerging Role in Cancer Therapy. *J Proteins proteomics*.
17. Hu C, et al. (2014) LXRα-mediated downregulation of FOXM1 suppresses the proliferation of hepatocellular carcinoma cells. *Oncogene* 33(22):2888–2897.
18. Teboul M, et al. (1995) OR-1, a member of the nuclear receptor superfamily that interacts with the 9-cis-retinoic acid receptor. *Proc Natl Acad Sci U S A* 92(6):2096–100.
19. Tang J, et al. Inhibiting macrophage proliferation suppresses atherosclerotic plaque inflammation. doi:10.1126/sciadv.1400223.
20. Gormally M V., et al. (2014) Suppression of the FOXM1 transcriptional programme via novel small molecule inhibition. *Nat Commun* 5:5165.
21. Marsico G, Gormally M V. (2015) Small molecule inhibition of FOXM1: How to bring a novel compound into genomic context. *Genomics Data* 3:19–23.
22. Robbins CS, et al. (2013) Local proliferation dominates lesional macrophage accumulation in atherosclerosis. *Nat Med* 19(9):1166–1172.
23. Tang J, et al. (2015) Inhibiting macrophage proliferation suppresses atherosclerotic plaque

inflammation. *Sci Adv* 1(3):e1400223–e1400223.

24. Lhoták Š, et al. (2016) Characterization of Proliferating Lesion-Resident Cells During All Stages of Atherosclerotic Growth. *J Am Heart Assoc* 5(8). Available at: http://jaha.ahajournals.org/content/5/8/e003945 [Accessed April 4, 2017].
25. Kojima Y, Weissman IL, Leeper NJ (2017) The Role of Efferocytosis in Atherosclerosis. *Circulation* 135(5):476–489.
26. Kojima Y, et al. (2016) CD47-blocking antibodies restore phagocytosis and prevent atherosclerosis. *Nature* 536(7614):86–90.
27. Moore KJ, Sheedy FJ, Fisher EA (2013) Macrophages in atherosclerosis: a dynamic balance. *Nat Rev Immunol* 13(10):709–721.
28. Jenkins SJ, et al. (2011) Local Macrophage Proliferation, Rather than Recruitment from the Blood, Is a Signature of TH2 Inflammation. *Science (80-)* 332(6035):1284–1288.
29. Sakai M, et al. (1996) The scavenger receptor serves as a route for internalization of lysophosphatidylcholine in oxidized low density lipoprotein-induced macrophage proliferation. *J Biol Chem* 271(44):27346–27352.
30. Flaveny CA, et al. (2015) Broad Anti-tumor Activity of a Small Molecule that Selectively Targets the Warburg Effect and Lipogenesis. *Cancer Cell* 28:42–56.
31. Solt LA, Kamenecka TM, Burris TP (2012) LXR-mediated inhibition of CD4+ T helper cells. *PLoS One* 7(9):e46615.
32. Pascual-Garcia M, et al. (2011) Liver X Receptors Inhibit Macrophage Proliferation through Downregulation of Cyclins D1 and B1 and Cyclin-Dependent Kinases 2 and 4. *J Immunol* 186(8):4656–4667.
33. Bensinger SJ, et al. (2008) LXR Signaling Couples Sterol Metabolism to Proliferation in the Acquired Immune Response. *Cell* 134(1):97–111.
34. Fukuchi J, Kokontis JM, Hiipakka RA, Chuu C, Liao S (2004) Antiproliferative effect of liver X receptor agonists on LNCaP human prostate cancer cells. *Cancer Res* 64(21):7686–7689.
35. Vedin L-L, Lewandowski SA, Parini P, Gustafsson J-Å, Steffensen KR (2009) The oxysterol receptor LXR inhibits proliferation of human breast cancer cells. *Carcinogenesis* 30(4):575–579.
36. Uno S, et al. (2009) Suppression of β-catenin signaling by liver X receptor ligands. *Biochem Pharmacol* 77(2):186–195.
37. Wang J zhong, Fang Y, Ji W dong, Xu H (2017) LXR agonists promote the proliferation of neural progenitor cells through MEK-ERK pathway. *Biochem Biophys Res Commun* 483(1):216–222.
38. Zhang X, et al. (2012) Cholesterol metabolite, 5-cholesten-3β-25-diol-3-sulfate, promotes hepatic proliferation in mice. *J Steroid Biochem Mol Biol* 132(3–5):262–270.

39. Teh M-T, et al. (2002) FOXM1 is a downstream target of Gli1 in basal cell carcinomas. *Cancer Res* 62(16):4773–80.
40. Chan DW, et al. (2008) Over-expression of FOXM1 transcription factor is associated with cervical cancer progression and pathogenesis. *J Pathol* 215(3):245–52.
41. Curtis C, et al. (2012) The genomic and transcriptomic architecture of 2,000 breast tumours reveals novel subgroups. *Nature* 486(7403):346–52.
42. Wang I-C, et al. (2008) Transgenic expression of the forkhead box M1 transcription factor induces formation of lung tumors. *Oncogene* 27(30):4137–4149.
43. Wierstra I (2013) The transcription factor FOXM1 (Forkhead box M1): Proliferation-specific expression, transcription factor function, target genes, mouse models, and normal biological roles. *Adv Cancer Res* 118:97–398.
44. Korver W, Roose J, Wilson A, Clevers H (1997) The Winged-Helix Transcription Factor Trident is Expressed in Actively Dividing Lymphocytes. *Immunobiology* 198(1–3):157–161.
45. Korver W, et al. (1997) The HumanTRIDENT/HFH-11/FKHL16Gene: Structure, Localization, and Promoter Characterization. *Genomics* 46(3):435–442.
46. Ye H, et al. (1997) Hepatocyte nuclear factor 3/fork head homolog 11 is expressed in proliferating epithelial and mesenchymal cells of embryonic and adult tissues. *Mol Cell Biol* 17(3):1626–41.
47. Down CF, Millour J, Lam EWF, Watson RJ (2012) Binding of FoxM1 to G2/M gene promoters is dependent upon B-Myb. *Biochim Biophys Acta - Gene Regul Mech* 1819(8):855–862.
48. Tanaka S, et al. (2016) BubR1 Insufficiency Results in Decreased Macrophage Proliferation and Attenuated Atherogenesis in Apolipoprotein E-Deficient Mice. *J Am Heart Assoc* 5(9):e004081.
49. Weidmann H, et al. (2015) SASH1, a new potential link between smoking and atherosclerosis. *Atherosclerosis* 242(2):571–579.
50. Gallagher KA, et al. (2015) Epigenetic changes in bone marrow progenitor cells influence the inflammatory phenotype and alter wound healing in type 2 diabetes. *Diabetes* 64(4):1420–30.
51. A-Gonzalez N, et al. (2009) Apoptotic cells promote their own clearance and immune tolerance through activation of the nuclear receptor LXR. *Immunity* 31(2):245–58.
52. Thorp E, Cui D, Schrijvers DM, Kuriakose G, Tabas I (2008) Mertk receptor mutation reduces efferocytosis efficiency and promotes apoptotic cell accumulation and plaque necrosis in atherosclerotic lesions of apoe-/- mice. *Arterioscler Thromb Vasc Biol* 28(8):1421–8.
53. Tanaka T, Terada M, Ariyoshi K, Morimoto K (2010) Monocyte chemoattractant protein-

1/CC chemokine ligand 2 enhances apoptotic cell removal by macrophages through Rac1 activation. *Biochem Biophys Res Commun* 399(4):677–682.

54. Bolick DT, et al. (2009) G2A deficiency in mice promotes macrophage activation and atherosclerosis. *Circ Res* 104(3):318–327.
55. Hanayama R, et al. (2002) Identification of a factor that links apoptotic cells to phagocytes. *Nature* 417(6885):182–187.
56. Ait-Oufella H, et al. (2007) Lactadherin deficiency leads to apoptotic cell accumulation and accelerated atherosclerosis in mice. *Circulation* 115(16):2168–2177.
57. Muse ED, et al. (2018) Cell-specific discrimination of desmosterol and desmosterol mimetics confers selective regulation of LXR and SREBP in macrophages. *Proc Natl Acad Sci*. doi:10.1073/pnas.1714518115.
58. Pineda-Torra I, Gage M, de Juan A, Pello OM (2015) Isolation, Culture, and Polarization of Murine Bone Marrow-Derived and Peritoneal Macrophages. *Methods Mol Biol* 1339:101–9.

FIGURE LEGENDS

Figure 1. M-S196A$^{Ldlr\text{-}KO}$ mice develop increased atherosclerosis on a Western diet. (**A**) (*Left*) En face Oil Red O-stained whole aortas (n=8-11/group), representative images shown. (*Right*) Quantification of stained areas as % plaque coverage for each genotype. (**B**) Haemotoxylin and Eosin (H&E)-stained aortic roots (n=9-10/group), scale bar at 500 μm representative images shown. (**C**) Quantification of stained areas as % plaque coverage for each genotype. (**D**) CD68 staining of aortic roots (n=7-8/group). Data are means ± SEM. *p<0.05, relative to WT$^{Ldlr\text{-}KO}$.

Figure 2. Changes in LXRα phosphorylation reprogram macrophage gene expression. (**A**) Volcano plot of $\log_2$ ratio vs p-value of differentially expressed genes comparing 12 week WD-fed M-S196A$^{Ldlr\text{-}KO}$ to WT$^{Ldlr\text{-}KO}$ BMDM (n=3/group). Blue line indicates adjusted p-value threshold of 0.04 (Wald Test for logistic regression. (**B**) Clustered heatmap of RNAseq gene counts in WD-fed macrophages (n=3 mice/group). (**C**) GSEA analysis showing enriched pathways in M-S196A$^{Ldlr\text{-}KO}$ macrophages derived from HALLMARK gene sets. (**D**) Fold-change of RNAseq gene counts in M-S196A$^{Ldlr\text{-}KO}$ compared to WT$^{Ldlr\text{-}KO}$ (set as 1) (n=3/genotype) for top induced genes (≥2-fold expression, p ≤0.01) involved in cell proliferation. (**E**) Heatmap of RNAseq gene counts of immune response genes downregulated by S196A in WD-fed macrophages (n=3 mice/group). (**F**) Heatmap of RNAseq gene counts of *(Top)* chemokine receptor and *(Bottom)* chemokine ligand genes showing differentially expressed genes in S196A WD-fed macrophages (n=3 mice/group). For all heatmaps blue and orange depicts upregulated and downregulated genes respectively and only genes showing ≥1.3-fold change with p ≤0.01 are shown.

Figure 3. Impaired macrophage LXRα phosphorylation induces FoxM1 expression and increases plaque cell proliferation. (**A**) Fold-change of RNAseq gene counts in WD-fed M-S196A$^{Ldlr\text{-}KO}$ compared to WD-fed WT$^{Ldlr\text{-}KO}$ macrophages (set as 1) for FoxM1 and FoxM1 target genes with ≥1.3-fold expression, p ≤0.01, n=3/genotype. **(B-D)** LXR occupancy and H3K27 acetylation (K27Ac) at the **(B)** *Srebf1* reported LXRE and **(C)** *FoxM1* and **(D)** *Cenpf* identified DR4 sequences (LXR binding sites) in BMDMs from M-S196A$^{Ldlr\text{-}KO}$ and WT$^{Ldlr\text{-}KO}$ WD-fed mice. Data shown normalized to input compared to a region within in a gene desert (Neg S) as a negative control. Shown is a representative experiment of 3 (each using n=2 mice/genotype). (**E**) Representative images of plaques exhibiting Ki67 positive nuclei, scale bar at 250 μm. (**F**) Quantification of Ki67 positive nuclei in WD-fed WT$^{Ldlr\text{-}KO}$ and M-S196A$^{Ldlr\text{-}KO}$ plaques (n= 6-10 mice/group). (**G**) *Left,* flow cytometry histograms of Ki67 expression in F4/80^{+} macrophages and *right,* bar chart of percentage of Ki67^{+} cells in WT^{LdlrKO} and M-S196A^{LdlrKO} macrophages exposed to 20μM FDI-6 inhibitor. Data shown is representative of three independent experiments (n=2 mice/genotype each). (**H**) *Left,* histogram and *right,* bar chart of percentage of Ki67^{+} M-S196A^{LdlrKO} macrophages in response to indicated concentrations of FDI-6. Data shown is representative of three independent experiments (n=2 mice/genotype each). (**I**) RT-qPCR analysis of FoxM1 target genes in WT^{LdlrKO} and M-S196A^{LdlrKO} macrophages. Normalised data shown relative to WT^{LdlrKO} as mean ± SD, n=3, (a) compared to WT-DMSO, (b) compared to M-S196A-DMSO.

Figure 4. M-S196A$^{Ldlr\text{-}KO}$ mice show decreased plaque necrotic cores and increased efferocytosis capacity. (**A**) (*Left*) H&E-stained mature plaques 'NC' depicts necrotic core (n= 4-6/group), representative images shown, scale bar at scale bar at 250 μm. (*Right*) Quantification of H&E-stained areas for each genotype. (**B**) Engulfment of apoptotic Jurkat cells (n=6/group). (**C**) Fold-change of RNAseq gene counts in WD-fed M-S196A$^{Ldlr\text{-}KO}$ compared to WD-fed WT$^{Ldlr\text{-}KO}$ macrophages (set as 1) for pro- and anti-phagocytic genes, p ≤0.01 n=3/genotype.

Figure 5. Macrophage transcriptional reprogramming in response to changes in LXRα phosphorylation is fundamentally different from ligand activation responses. (**A,B**) RNAseq analysis on M-S196A$^{Ldlr\text{-}KO}$ and WT$^{Ldlr\text{-}KO}$ macrophages from WD-fed mice exposed to 1μM GW3965 (GW) (n=3/group). Venn diagram of genes (**A**) induced or (**B**) reduced in S196A compared to WT cells. (**C**) Comparison of ligand responses in M-S196A$^{Ldlr\text{-}KO}$ and WT$^{Ldlr\text{-}KO}$ macrophages. (Center) Venn diagram of genes induced (UP) or reduced (DOWN) by GW in LXRαWT cells compared to differentially expressed genes (DEGs) in S196A vs WT in vehicle-treated (DMSO) conditions. Bar graphs show fold changes in gene expression for genes (Top) induced or (Bottom) reduced by GW that are also differentially regulated by S196A. (**D**) Clustered

heatmap of RNAseq gene counts for FoxM1 and its target genes in macrophages from WD-fed mice (n=3/group) treated as indicated. (**E**) RT-qPCR analysis of *FoxM1* and its target genes in WD-fed $WT^{Ldlr\text{-}KO}$ and M-S196A$^{Ldlr\text{-}KO}$ macrophages. Normalized data shown relative to $WT^{Ldlr\text{-}KO}$ as mean ± SD, n=3, (a) p≤0.001 compared to WT-DMSO, (b) p≤0.001 compared to S196A-DMSO, (c) p≤0.001 compared to WT-GW. (**F**) mRNA expression of *FoxM1* regulators. Data and statistical analysis as in E.

SI Materials and Methods

Mice

The S196A floxed ($S196A^{fl/fl}$) mouse line was generated by Ozgene Pty Ltd (Bentley WA, Australia). The genomic sequence for the murine LXRα (Nr1h3) gene was obtained from the Ensembl Mouse Genome Server (http://www.ensembl.org/Mus_musculus/), Ensembl gene ID: ENSMUSG00000002108. The mutant fragment, located on Exon 5, contains a serine-to-alanine mutation at Ser196 introduced by site-directed mutagenesis. The point-mutant exon was delivered into an intronic site inside the targeting vector, placed in opposite orientation and thus without coding capacity (Fig. S1A). The targeting construct was electroporated into the Bruce4 C57BL/6 ES cell line. Homologous recombinant ES cell clones were identified by Southern hybridization and injected into BALB/cJ blastocysts. Male chimeric mice were obtained and crossed to C57BL/6J females to establish heterozygous germline offsprings on a pure C57BL/6 background. The germline mice were crossed to a FLP Recombinase mouse line(1) to remove the FRT flanked selectable marker cassette (Flp'd mice ($Flp^{+/+}$). $Flp^{+/+}$ mice are homozygous for FL allele containing LXRα WT exon 5 (Ex5) and LXRα S196A exon 5 of the LXRα gene in opposite orientation flanked by lox sites sensitive to Cre recombinase activity. These mice express LXRα WT but switch to LXRα S196A expression in the presence of CRE recombinase. $Flp^{+/+}$ mice were crossed with (1) a C57BL/6 homozygous Ldl receptor null ($Ldlr^{-KO}$) mouse strain, to generate a $Flp^{+/+}Ldlr^{-KO}$ strain and (2) a C57BL/6 homozygous LysMCre ($LysMCre^{+/+}$) strain to generate a $Flp^{+/+}LysMCre^{+/-}$ strain. The two resulting lines were then crossed to generate $Flp^{+/+}Ldlr^{-KO}LysMCre^{+/-}$. Cre recombinase expression under direction of the LysM promoter in $Flp^{+/+}Ldlr^{-KO}LysMCre^{+/-}$ results in the switch to LXRα S196A expression in myeloid cells, these mice ($M\text{-}S196A^{Ldlr\text{-}KO}$) were compared to littermate non- CRE expressing mice ($Flp^{+/+}Ldlr^{-KO}LysMCre^{-/-}$ or $WT^{Ldlr\text{-}KO}$) which were used as controls in our study. The Ldlr-KO and LysMCre strains were purchased from The Jackson Laboratory (stock numbers 002207 and 004781, respectively)

Animals were housed together and maintained in a pathogen-free animal facility in a 12-h light-12h dark cycle. All procedures were carried under the UK's Home Office Animals (Scientific Procedures) Act 1986.

Genotyping

Mice were genotyped by PCR analysis of ear biopsies using Jumpstart Taq DNA Polymerase (Sigma Aldrich) and the following primers: For S198A knock-in, primers R2 and WT identify the wild-type allele (642bp) and FL allele (656bp), primers R2 and SA identifly the mutant allele of LXRα S196A knock-in mice (656 bp): SA 5' GGTGTCCCCAAGGGTGTCCG wild-type 5' GGTGTCCCCAAGGGTGTCCT, R2 5' AAGCATGACCTGCACACAAG, Ldlr; oIMR0092 (mutant): 5' AATCCATCTTGTTCAATGGCCGATC, oIMR3349 (common): 5' CCATATGCATCCCCAGTCTT, oIMR3350 (wild-type): 5' GCGATGGATACACTCACTGC,

LysMcre; oIMR3066 (mutant): 5' CCCAGAAATGCCAGATTACG, oIMR3067 (common): 5' CTTGGGCTGCCAGAATTTCTC, oIMR3068 (wild-type): 5' TTACAGTCGGCCAGGCTGAC.

Diet induced atherosclerosis

Eight-week old $WT^{Ldlr\text{-}KO}$ and $M\text{-}S196A^{Ldlr\text{-}KO}$ male mice were fed ad libitum a Western diet (WD) (20% Fat, 0.15% Cholesterol; #5342 AIN-7A, Test Diet Limited, UK) for 12 weeks. Mice were fasted overnight prior to sacrifice.

Metabolic tests

Blood was sampled from saphenous vein as previously described(2). Glucose concentrations were determined in whole blood by a portable meter (Roche Diagnostics, 2 Burgess Hill, UK). Plasma insulin concentrations were determined by enzyme-linked immunoassay (#EZRMI-13K, Merck Millipore). Plasma total cholesterol and triglyceride levels (Wako Diagnostics), as well as NEFAs (Abcam), were determined by colorimetric enzymatic assay kits as per the manufacturer's recommendations.

Atherosclerosis quantification

***En face* analysis of aorta.** Mice were perfusion-fixed with phosphate-buffered paraformaldehyde (4% [wt/vol.], pH 7.2) under terminal anaesthesia. The entire aortic tree was dissected free of fat and other tissue. Aortae were stained with oil red O and mounted onto glass slides before imaging (Leica, DFC310FX) under a dissection microscope (Leica, MZ10F). Lesion area of whole aorta was analysed using Image J.

Aortic sinus. Hearts were formalin-fixed, paraffin-embedded and 5 µm aortic sinus sections were stained with stained with hematoxylin and eosin (H&E). Stained sections were scanned with NanoZoomer Digital slide scanner (Hamamatsu). Percentage atherosclerotic lesion were determined using Image J by averaging 3 sections from each mouse with 30-50 µm intervals between sections(2).

Macrophage content. Immunohistochemistry staining was performed at the UCL IQPath Laboratory using the Ventana Discovery XT instrument, using the Ventana DAB Map detection Kit (760-124). For pre-treatment Ventana Protease 1 (equivalent to pronase, 760-2018) was used. CD68 primary antibody (AbD Serotec #MCA1957), followed by Rabbit anti Mouse (#E0354 Dako). Stained sections were scanned with NanoZoomer Digital slide scanner (Hamamatsu). Macrophage content was quantified in the plaque using Image J.

Plaque complexity. Percent necrotic core was measured in H&E stained aortic roots as acellular area(3) using Image J.

Cell culture

Bone marrow derived macrophage culture. Bone Marrow-derived Macrophages (BMDM) were prepared as in(4) using L929 Conditioned Medium (LCM) as a source of M-CSF for the differentiation of the macrophages. After 6 days of differentiation, LCM-containing medium was removed, cells were washed three times in warm PBS and incubated in DMEM containing low-endotoxin (≤10 EU/mL) 1% FBS and 20 µg/mL gentamycin without any LCM before being treated with DMSO or 1 µmol/L GW3965 (Tocris) for 24 hrs. For inhibitor experiments, 5 days post-differentiation, LCM-containing medium was removed, cells washed three times with warm PBS and incubated with DMEM containing low endotoxin (≤10 EU/mL) 10% FBS and 20 µg/mL gentamycin without any LCM before being treated with DMSO or FDI-6 (#1392, Sigma) at indicated concentrations for 24 (mRNA quantification) or 48 hours (flow cytometry).

Isolation of mouse peritoneal macrophages. Peritoneal macrophages were harvested 4 days after i.p. injection of 4% thioglycolate by peritoneal lavage. Macrophages were seeded at $2x10^6$ cells/mL in RPMI and adherent macrophages were washed in PBS and harvested after 2 hours.

Jurkat culture. Jurkat cells were cultured in RPMI supplemented with 10% FBS and passaged every two days to maintain a cell concentration not exceeding $1x10^6$ cells/mL.

RAW 264.7 culture. RAW-LXRα and RAW-S198A cells expressing receptors were cultured as decribed(5).

Efferocytosis

Jurkat cells or BMDM were labeled for 1 hr with calcein AM and apoptosis was induced by UV irradiation. Apoptotic cells were added to monolayers of BMDM at a ratio of 1:1. After 30 min of co-culture, non-ingested apoptotic cells were removed, and slides fixed in 1% PFA. Images were captured (microscope: Zeiss Axio Vert.A1, camera: Zeiss Axiocam 503 mono) and ingested apoptotic cells quantified as in(6) using Image J.

Ki67 Staining by flow cytometry

Macrophages were washed with PBS before incubation with dissociation media (PBS + 10µM EDTA + 4mg/mL lidocaine + Pen/Strep) at 37°C for 15 minutes and removal from tissue culture plates by gentle scraping. Cells were stained with a Zombie™ Fixable Viability Dye (BioLegend), followed by anti-Mouse F4/80-FITC (Clone BM8, eBioscience™), then fixed and permeabilised using eBioscience™ Fixation/Permeabilisation reagents (Invitrogen). Intracellular staining with PE Mouse anti-Ki67 Set (BD Pharmingen™) was performed in eBioScience™ Permeabilisation Buffer (Invitrogen) for 30 minutes at 4°C. Samples were acquired on a BD LSR Fortessa™ X-20 (BDBioscience) using BD FACSDiva™ Software. Data was analysed using FlowJo® v10.4 (Tree Star Inc.)

Monocytosis

Blood samples were obtained by cardiac puncture. Red blood cells were lysed for 17s in distilled water, followed by a second lysis using ACK lysis buffer (Lonza). Cells were washed once in cell staining buffer, stained with Zombie^{TM} Fixable Viability Dye (BioLegend), followed by surface staining with anti-Mouse CD45-BV510 (clone 30-F11, BD Biosciences), CD11b- PerCP Cy5.5 (clone M1/70, eBioscience) and CD115-PE (clone AFS98, BioLegend). Cells were washed in cell staining buffer and resuspended in 0.5% PFA with CountBright absolute counting beads (ThermoFisher).

RNA extraction and quantification

Total RNA from was extracted with TRIzol Reagent (Invitrogen). Sample concentration and purity was determined using a NanoDrop™ 1000 Spectrophotometer and cDNA was synthesized using the qScript cDNA Synthesis Kit (Quanta). Specific genes were amplified and quantified by quantitative Real Time-PCR, using the PerfeCTa SYBR Green FastMix (Quanta) on an MX3000p system (Agilent). Primer sequences are shown in supplementary table S5. The relative amount of mRNAs was calculated using the comparative Ct method and normalized to the expression of cyclophylin(7).

Protein isolation and immunoblotting

Total cellular protein lysates (30µg) or nuclear extracts were loaded onto a 10% SDS-PAGE gel, electrophoresed and transferred onto a PVDF membrane. Membranes were probed with anti-LXRα (ab41902, Abcam), phospho-Ser196 specific rabbit polyclonal antibody (8), and anti-Hsp90 (sc-7947, Santa Cruz) overnight in 2.5% BSA, TBS, followed by incubation with anti-rabbit (PO448, Dako) or anti-mouse (NA931VS, GE Healthcare) horseradish-peroxidase-tagged antibodies. Chemiluminescence (ECL 2 Western Blotting Substrate, Pierce) was used to visualise proteins.

RNA sequencing and analysis

Total RNA was extracted using TRIzol reagent (Life technologies) and cDNA libraries were prepared using reagents and protocols supplied with the Stranded mRNA-Seq Kit (Kapa Biosystems). Briefly, poly-A tailed RNA was purified using paramagnetic oligo-dT beads from 200 nanograms of total RNA, with a RNA Integrity Number above 7.5 as determined by the Agilent Bioanalyzer (Agilent). The purified RNA was chemically fragmented and cDNA was synthesised using random primers (Kapa Biosystems). Adapter-ligated DNA library was amplified with 12

cycles of PCR and library fragment was estimated using the Agilent TapeStation 2200.Library concentration was determined using the Qubit DNA HS assay (Life Technologies). Libraries were sequenced on an Illumina NextSeq 500, NCS v2.1.2 (Illumina) with a 43bp paired end protocol. Basecalling was done using standard Illumina parameters (RTA 2.4.11). Sequencing and pipeline analysis was performed by UCL Genomics (London, UK) and using Partek Flow software. Reads were demulitplexed using Illumina bcl2fastq v2.17 (Illumina) and aligned using STAR v2.5.0b to the mouse GRCm38/mm10 reference sequence. Transcript abundance was estimated using Illumina's RnaReadCounter tool and differential expression analysis performed with DESeq2, which uses the Benjamin-Hochberg method for multiple testing correction (FDR< 0.05). Pathway enrichment analysis was performed with the Gene Set Enrichment Analysis (GSEA) software's preranked module(9, 10) or the GSEA module in the WebGestalt (http://www.webgestalt.org) analysis toolkit. Reactome pathway analysis was performed with WebGestalt using the Benjamini-Hochberg method to adjust p values for multiple testing and FDR <0.05. Heatmaps of gene counts were done with Heatmapper Expression tool(11) (http://www1.heatmapper.ca/expression/) and Venn diagrams using a BGE tool (http://bioinformatics.psb.ugent.be/webtools/Venn/). Dot and box plot graphs were generated using Partek Flow software.

ChIP-sequencing

Immortalized bone marrow derived-macrophages (iBMDM) from LXRαβ$^{-/-}$ mice have been described(12). N-terminus 3xFLAG-tagged LXRα or LXRβwere ectopically expressed in LXR-null iBMDM using a pBabe-puro retroviral expression system as described(13). A control LXRαβ$^{-/-}$ iBMDM line was also prepared by transduction with an empty pBabe-puro vector. For genome-wide binding analysis of LXR proteins, FLAG-tagged cells were cultured in DMEM supplemented with 1% FFA-free BSA, 50nM of Zaragozic acid (Squalene Synthase inhibitor; Sigma), and 1 uM of GW3965 LXR agonist or GW2033 LXR antagonist (both kindly provided by Jon Collins, Glaxo SmithKline) for 24 h. Immortalized bone marrow derived-macrophages (12 x 10^6) were crosslinked with 2mM DSG (disuccinimidyl glutarate) for 30 min and 1% methanol-free ultrapure formaldehyde for 10 min before quenching with 2 M Glycine. Cells were lysed with RIPA buffer and, after chromatin shearing by sonication (Bioruptor Diagenode), incubated overnight with protein G magnetic Dynabeads (Invitrogen) that were previously coupled with 3 µg of anti-FLAG M2 (Sigma) antibodies according to the manufacturer's instructions. Immunoprecipitated DNA was purified using Qiagen columns. For high-throughput sequencing, ds DNA was obtained by pooling DNA from 10 independent ChIP (for FLAG-LXR sequencing). DNA was then used for library preparation and subsequent Illumina HiSeq sequencing by the Centre de Regulació Genomica (CRG, Barcelona, Spain) genomic facility.

Chomatin immunoprecipitation

ChIP experiments were performed and analysed as described(7) except cells were cross-linked with 2mM of disuccinimidyl glutarate (Thermo Scientific) for 20 min, followed by 10 min with 1% formaldehyde solution (Thermo Scientific). The antibodies employed include: LXRα (#61176, Active Motif, 10μg) and H3K27ac (ab4729, Abcam, 3μg). Oligonucleotides used are shown in Supplementary Table S6. To control for non-specific binding, an 82 base pair fragment in a gene desert in chromosome 6 using commercial oligonucleotides (#71011,ActiveMotif) was used.

Statistics

Results are expressed as mean (SEM). Comparisons within groups were made using paired Students t-tests and between groups using unpaired Students t tests or repeated measures ANOVA, as appropriate; where repeated *t-tests* were performed a Bonferroni correction was applied. P≤0.05 considered statistically significant except for RNAseq analysis where P≤0.01 was used.

References

1. Takeuchi T, et al. (2002) Flp recombinase transgenic mice of C57BL/6 strain for conditional gene targeting. *Biochem Biophys Res Commun* 293(3):953–957.
2. Gage MC, et al. (2013) Endothelium-specific insulin resistance leads to accelerated atherosclerosis in areas with disturbed flow patterns: a role for reactive oxygen species. *Atherosclerosis* 230(1):131–9.
3. Feng B, et al. (2003) Niemann-Pick C heterozygosity confers resistance to lesional necrosis and macrophage apoptosis in murine atherosclerosis. *Proc Natl Acad Sci* 100(18):10423–10428.
4. Pineda-Torra I, Gage M, de Juan A, Pello OM (2015) Isolation, Culture, and Polarization of Murine Bone Marrow-Derived and Peritoneal Macrophages. *Methods Mol Biol* 1339:101–9.
5. Torra IP, et al. (2008) Phosphorylation of liver X receptor alpha selectively regulates target gene expression in macrophages. *Mol Cell Biol* 28(8):2626–36.
6. Thorp E, et al. (2011) Shedding of the Mer Tyrosine Kinase Receptor Is Mediated by ADAM17 Protein through a Pathway Involving Reactive Oxygen Species, Protein Kinase Cζ, and p38 Mitogen- activated Protein Kinase (MAPK) *. doi:10.1074/jbc.M111.263020.
7. Pourcet B, et al. (2011) LXRα regulates macrophage arginase 1 through PU.1 and interferon regulatory factor 8. *Circ Res* 109(5):492–501.
8. Torra IP, et al. (2008) Phosphorylation of liver X receptor alpha selectively regulates target gene expression in macrophages. *Mol Cell Biol* 28(8):2626–2636.

9. Mootha VK, et al. (2003) PGC-1α-responsive genes involved in oxidative phosphorylation are coordinately downregulated in human diabetes. *Nat Genet* 34(3):267–273.
10. Subramanian A, et al. (2005) Gene set enrichment analysis: a knowledge-based approach for interpreting genome-wide expression profiles. *Proc Natl Acad Sci U S A* 102(43):15545–50.
11. Babicki S, et al. (2016) Heatmapper: web-enabled heat mapping for all. *Nucleic Acids Res* 44(W1):W147–W153.
12. Ito A, et al. (2015) LXRs link metabolism to inflammation through Abca1-dependent regulation of membrane composition and TLR signaling. *Elife* 4:e08009.
13. Chen M, Bradley MN, Beaven SW, Tontonoz P (2006) Phosphorylation of the liver X receptors. *FEBS Lett* 580(20):4835–4841.

Supplementary Figure 1

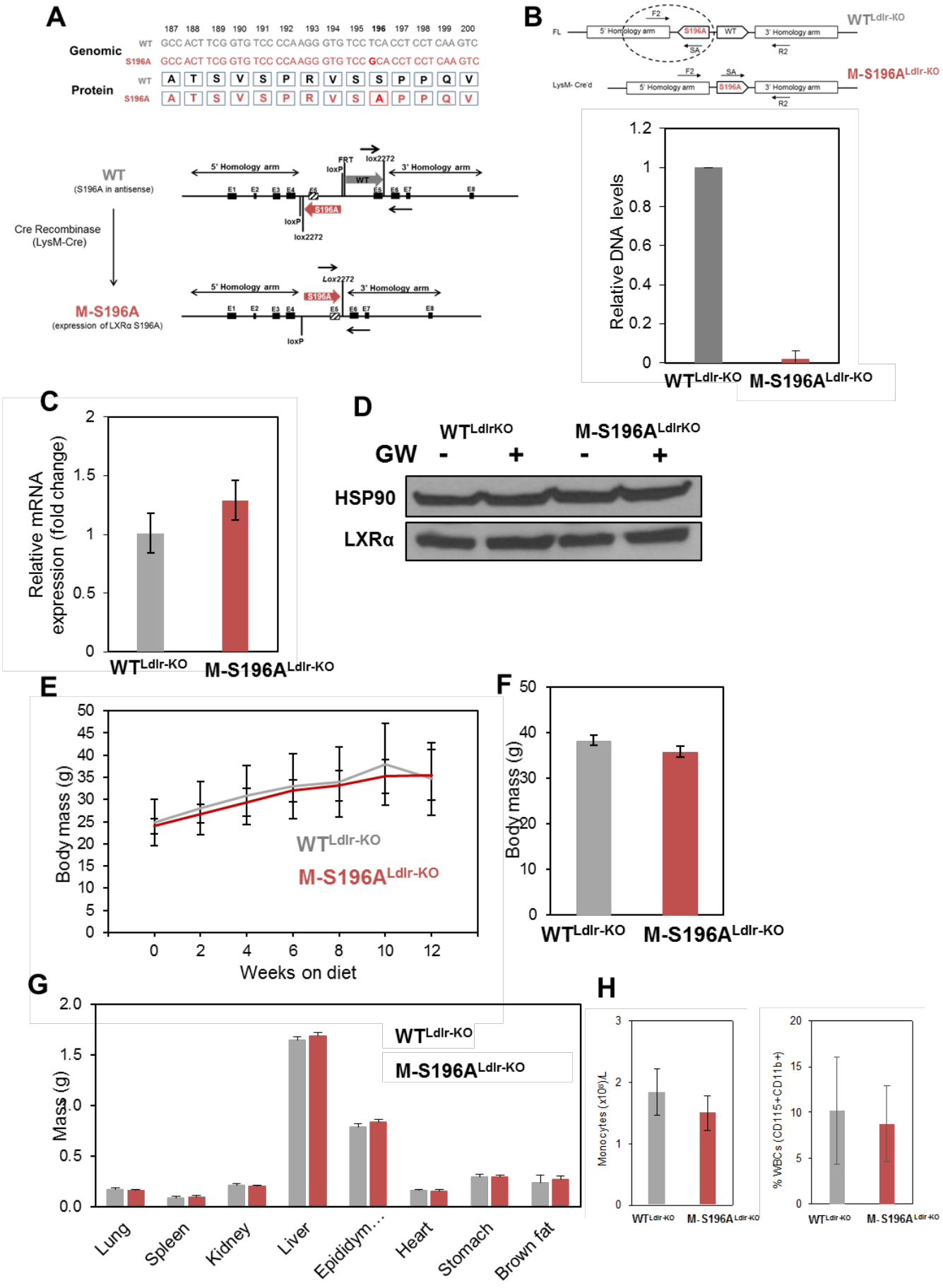

(**A**) *(Top)* WT and S196A genomic and protein sequence alignment of the murine LXRα depicting the single-site mutation at S196A. *(Bottom)* Schematic diagram illustrating the targeting construct used for the generation of M-S196A model and targeted loci. (**B**) Relative levels of $S196A^{FL/FL}$ (n=4 per group) for the quantification of cre-mediated recombination efficiency showing $M\text{-}S196A^{LdlR\text{-}KO}$ mice express the knock-in mutation in macrophages**.** Primer pair F2-SA selectively amplifies FL allele in $S196A^{fl/fl}$ (WT). (**C**) LXRα expression in BMDMs by RT-qPCR analysis (n=3/genotype). (**D**) LXRα protein expression in BMDMs by Western blot analysis. (**E**) Growth curve (n=8-11 per group). (**F**) Terminal body mass (n >20 mice per group). (**G**) Organ mass (n=8-11 per group). (**H**) (*Left*) Number of monocytes or (*Right*) percentage of white blood cells in blood (n=3 mice per genotype).

Supplementary Figure 2

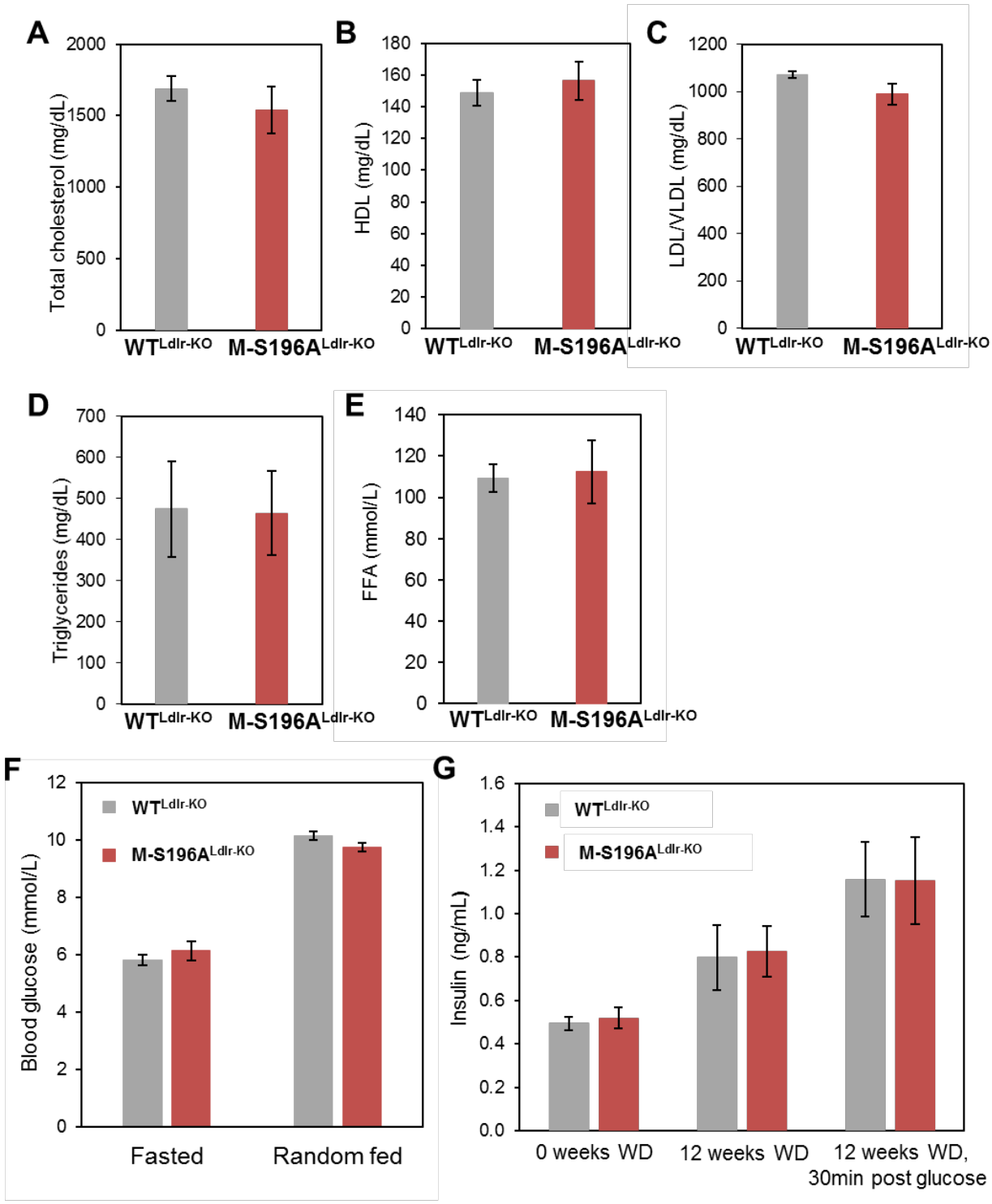

Plasma (**A**) total cholesterol, (**B**) HDL cholesterol, (**C**) LDL/VLDL cholesterol, (**D**) Triglycerides and (**E**) Free fatty acids. Blood (**F**) glucose and (**G**) insulin (n=6 -11 mice per group).

Supplementary Figure 3

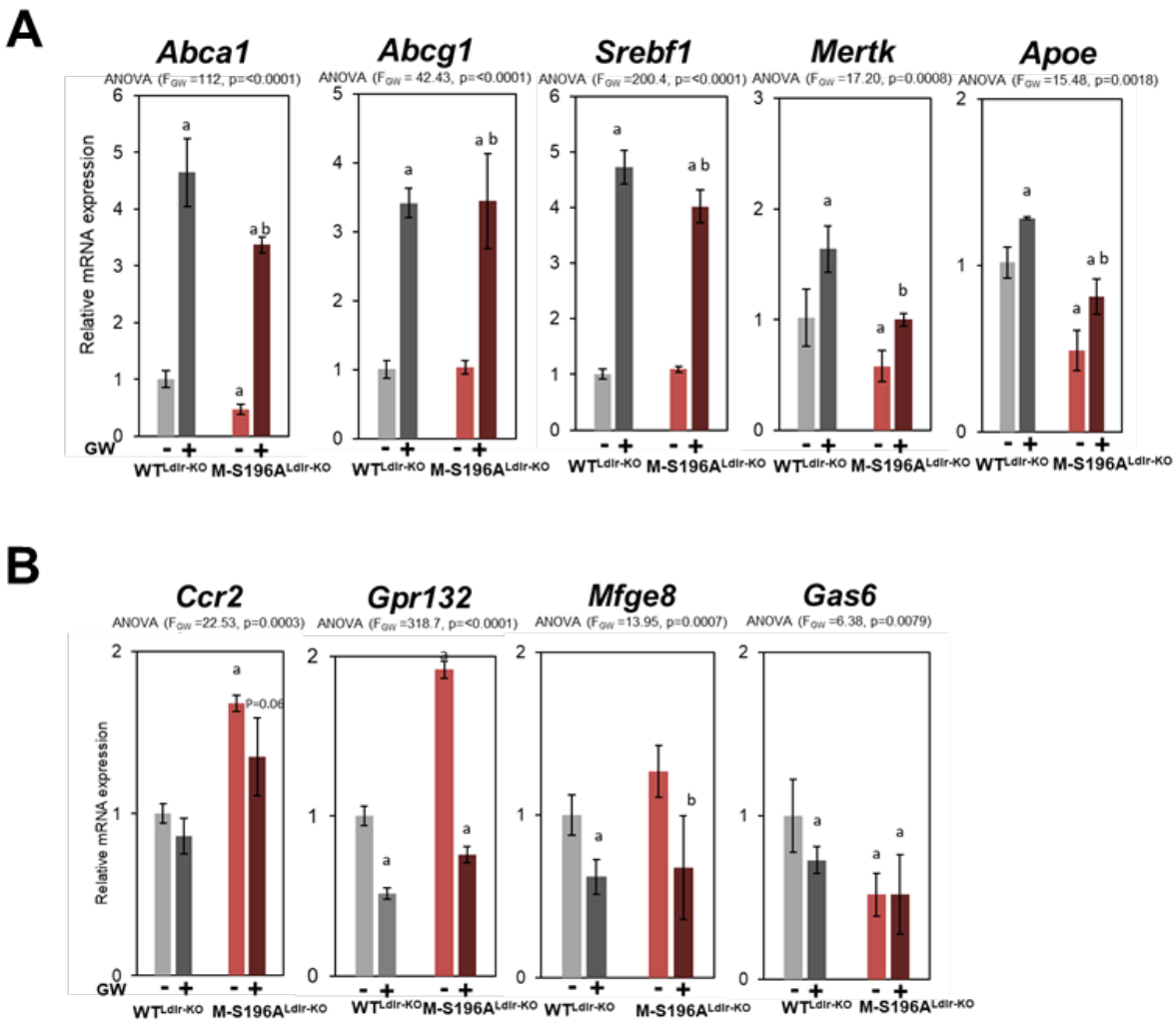

(A) RT-qPCR analysis of LXR targets in response to LXR activation by GW 3965 (GW) in WT^{LdlrKO} and $M\text{-}S196A^{LdlrKO}$ macrophages. (**B**) RT-qPCR analysis of a selection of genes with efferocytosis functions and respose to LXR activation by GW 3965 (GW) in WT^{LdlrKO} and $M\text{-}S196A^{LdlrKO}$ macrophages. Normalised data shown relative to WT^{LdlrKO} as mean ± SD, n=3, (a) compared to WT-DMSO, (b) compared to M-S196A-DMSO.

Supplementary Figure 4

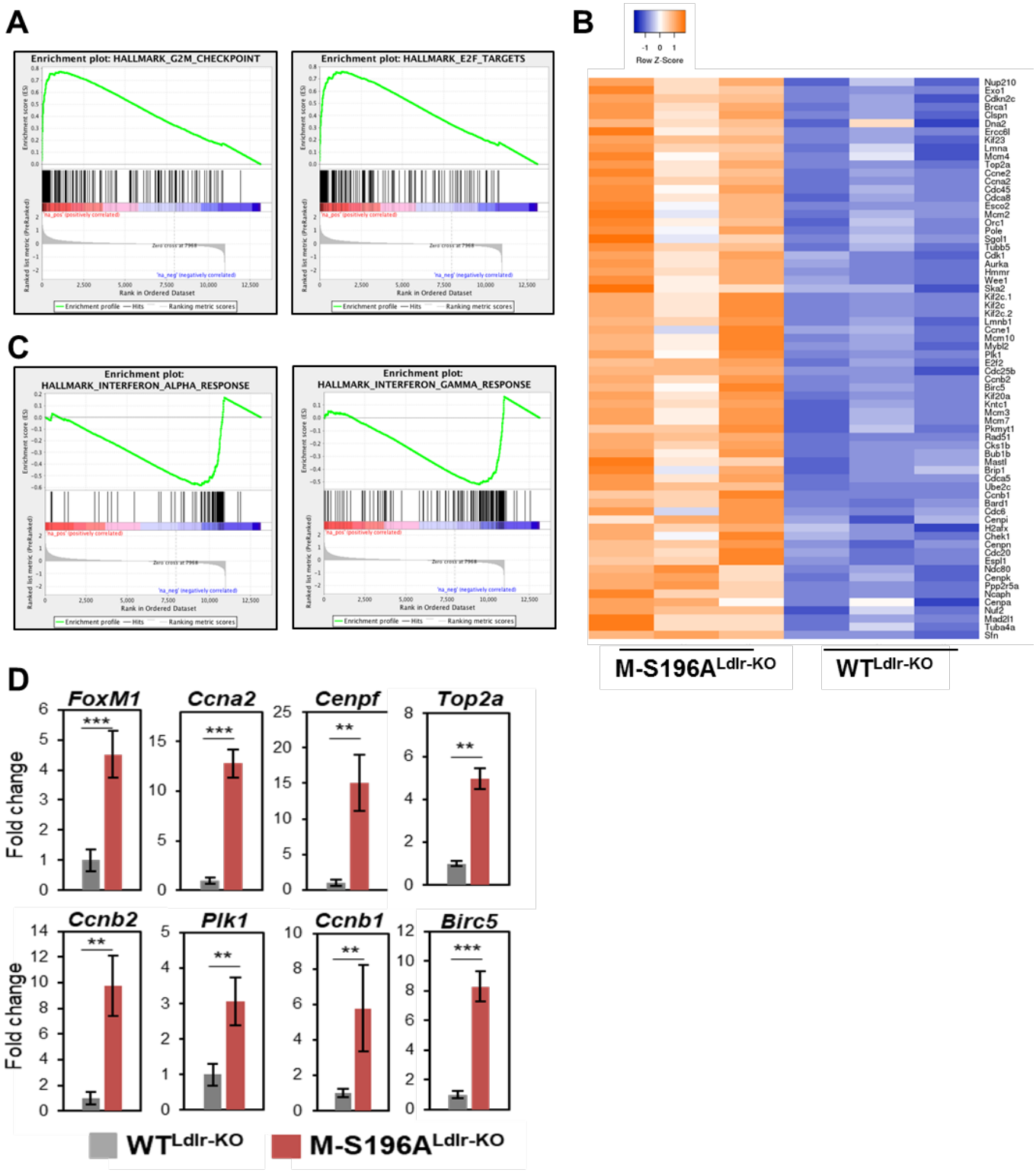

(**A**) Enrichment plots for top 2 induced Hallmark pathways in WD-fed M-S196A$^{Ldlr\text{-}KO}$ macrophages compared to WD-fed WT$^{Ldlr\text{-}KO}$. (**B**) Clustered heatmap of macrophage RNAseq gene counts of cell cycle and proliferation genes in WD-fed mice (n=3/genotype). (**C**) Enrichment plots for top 2 reduced Hallmark pathways in WD-fed M-S196A$^{Ldlr\text{-}KO}$ macrophages compared to WD-fed WT$^{Ldlr\text{-}KO}$. (**D**) RT-qPCR analysis of FoxM1 and top FoxM1 regulated targets in

WD-fed WT$^{Ldlr\text{-}KO}$ and M-S196A$^{Ldlr\text{-}KO}$ macrophages. Normalized data shown relative to WT$^{Ldlr\text{-}KO}$ (set as 1) as mean ± SEM, n=3, **p<0.01 or ***p<0.001.

Supplementary Figure 5

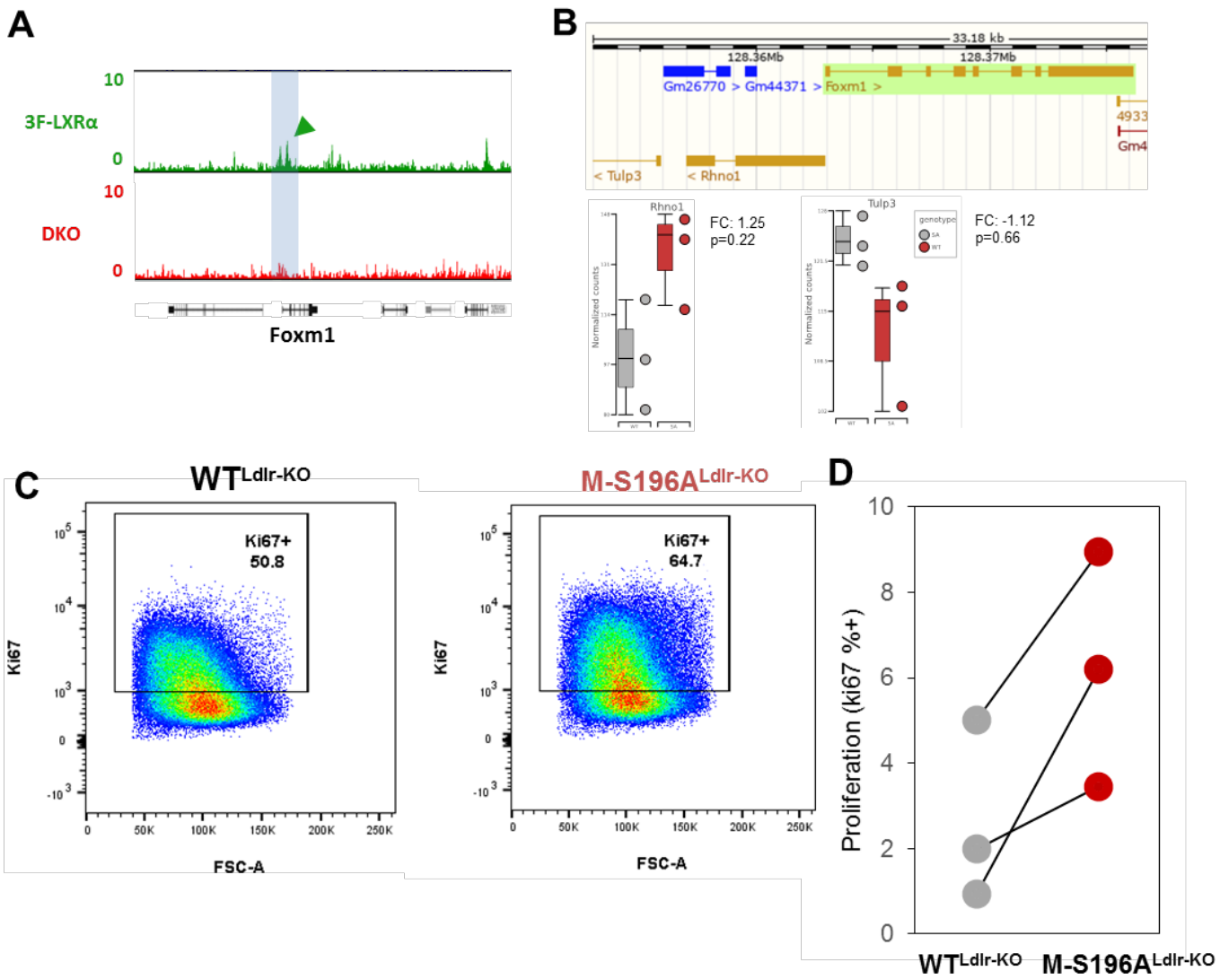

(**A**) ChIPseq LXRα track on LXR-deficient BMDMs (DKO, red tracks) or BMDMs overexpressing FLAG-tagged LXRa (green tracks) cells incubated with GW3965 ligand. Arrowheads point at identified peaks. (**B**) (Top) Screenshot depicting genes upstream of the FoxM1 locus. (Bottom) Box and dot plots of normalised gene counts for Rhno1 and Tulp3, located upstream of FoxM1. (**C**) FACS plots of Ki67 levels in WT$^{Ldlr\text{-}KO}$ and M-S196A$^{Ldlr\text{-}KO}$ macrophages. Shown is a representative experiment of 2. (**D**) Linked dot plots showing increased proliferation of M-S196A$^{Ldlr\text{-}KO}$ macrophages in three independent experiments, 1-2 mice/ genotype.

Supplementary Figure 6

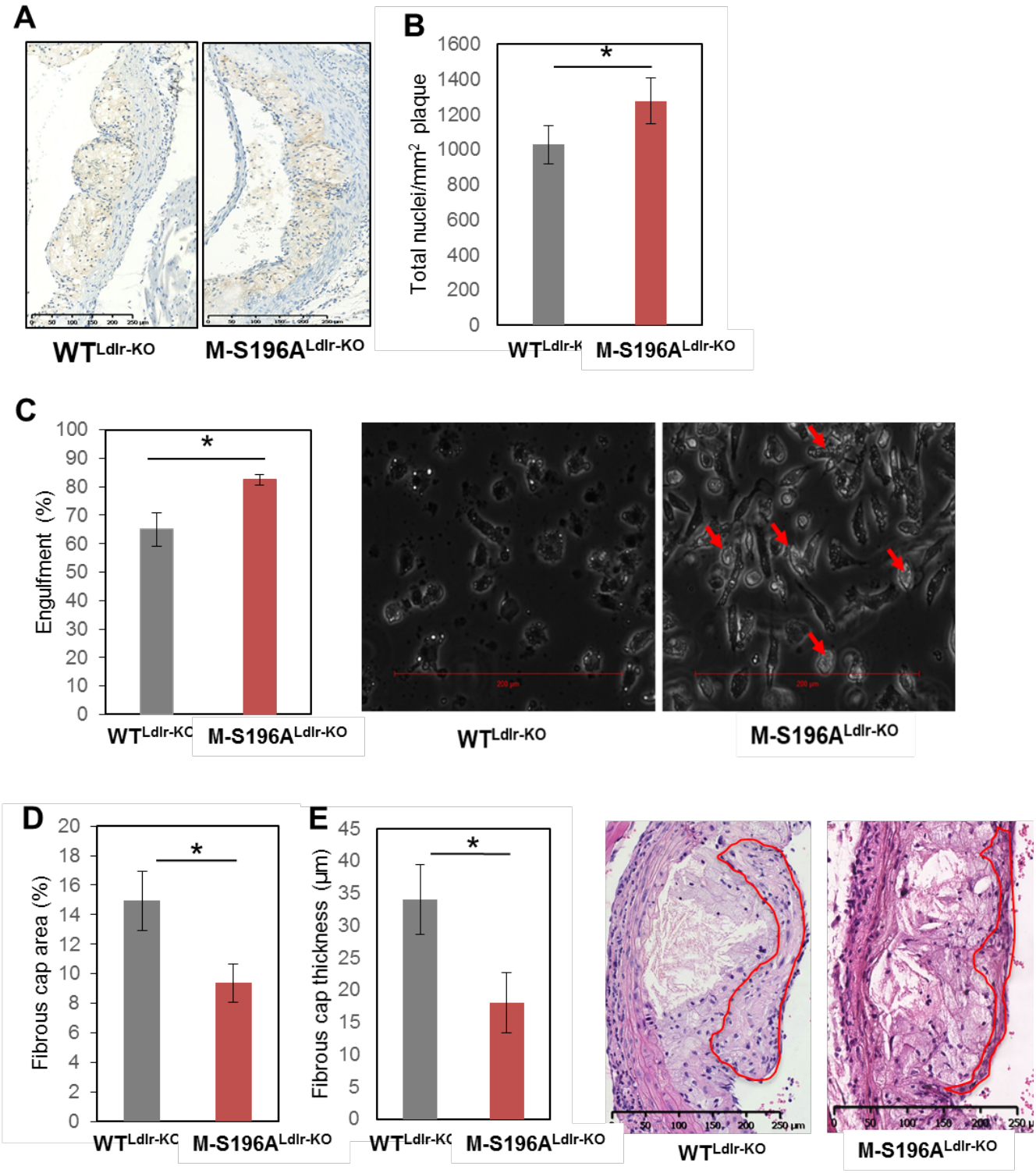

(**A**) Representative images of CD68 stained aortic root sections, scale bar at 250 µm. (**B**) Quantification of total number of nuclei per mm^2 of plaque from H&E-stained sections (n=6/ group). (**C**) (*Left*) Apoptotic macrophage (BMDMs) engulfment by $WT^{Ldlr\text{-}KO}$ or $M\text{-}S196A^{Ldlr\text{-}KO}$ macrophages (n=3/ group. (*Right*) Representative images for each genotype shown, scale bar at 200 µm. Shown is a representative experiment of 2 independent sets. (**D**) Fibrous cap area (% of total atherosclerotic lesion area) (n=6/ group) and (**E**) (*Left*) Fibrous cap thickness quantification (n=6/ group). (*Right*) Representative images of plaques with delineated fibrous caps in red, scale bar at 250µm. Data represents means ± SEM. * $p < 0.05$ relative to $WT^{Ldlr\text{-}KO}$ determined by Student's t-test.

Supplementary Figure 7

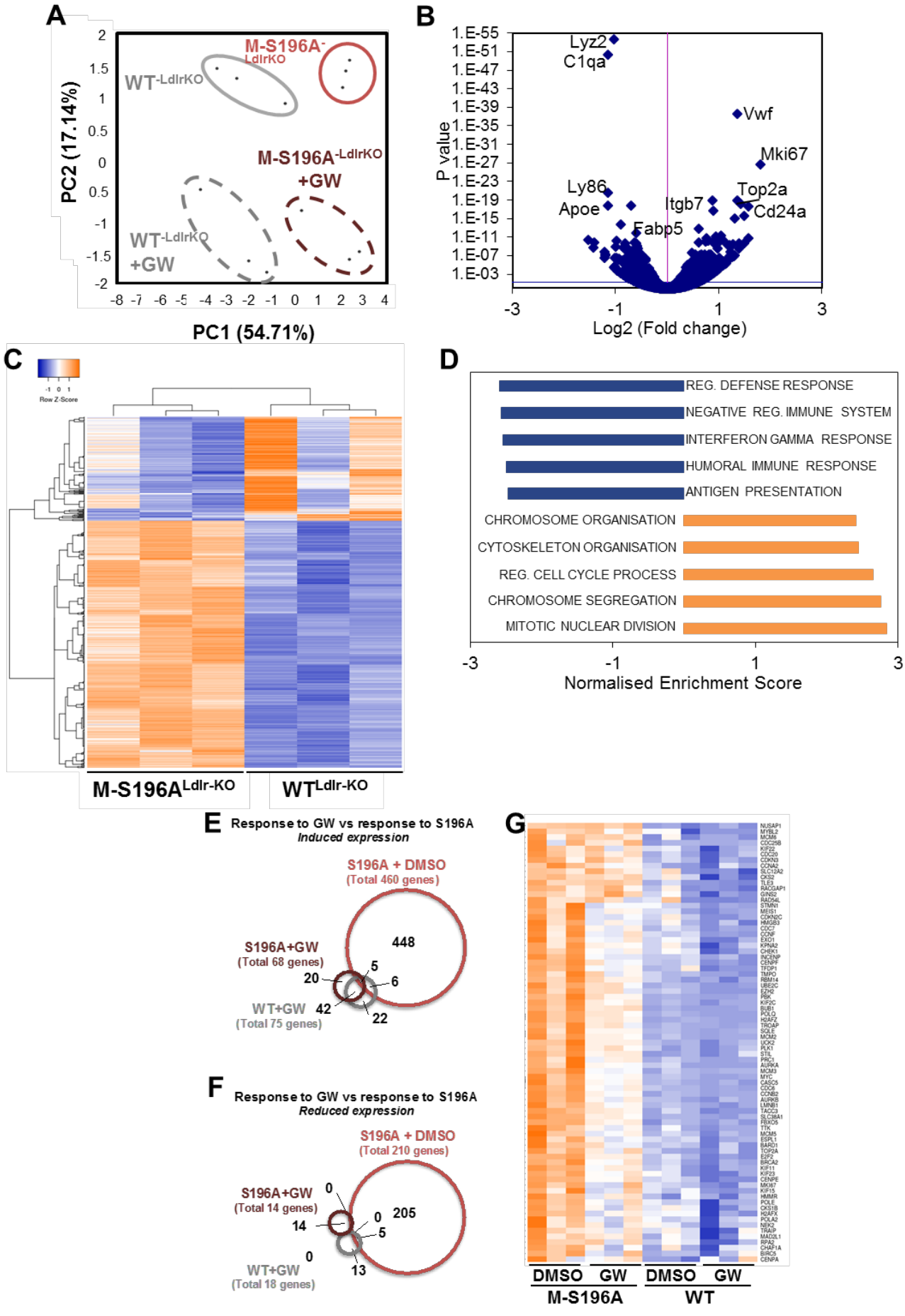

(**A**) Principal Component (PC) Analysis plot showing RNAseq samples from WD-fed mice analysed by genotype and ligand treatment (n=3/group). (**B**) Volcano plot of $\log_2$ ratio vs p-value of differentially expressed genes in GW3965-treated macrophages from WD-fed M-S196A$^{Ldlr\text{-}KO}$ compared to WT$^{Ldlr\text{-}KO}$ mice (n=3/group). Blue line indicates adjusted p-value threshold of 0.04. (**C**) Clustered heatmap of RNAseq gene counts in GW3965-treated macrophages from WD-fed mice (n=3/group) showing genes that exhibit ≥1.3-fold expression, p ≤0.01 over ligand-treated WT$^{Ldlr\text{-}KO}$ cells. (**D**) GSEA analysis showing enriched pathways in M-S196A$^{Ldlr\text{-}KO}$ macrophages incubated with 1μM GW3965 compared to ligand-treated WT$^{Ldlr\text{-}KO}$ cells. (**E, F**) RNAseq analysis on M-S196A$^{Ldlr\text{-}KO}$ and WT$^{Ldlr\text{-}KO}$ macrophages from WD-fed mice exposed to 1μM GW3965 (GW) (n=3/group). Venn diagram of genes (**F**) induced or (**G**) reduced in S196A compared to WT cells. (**G**) Clustered heatmap of RNAseq gene counts of G2M checkpoint genes in macrophages from WD-fed mice (n=3/group).

Supplementary Figure 8

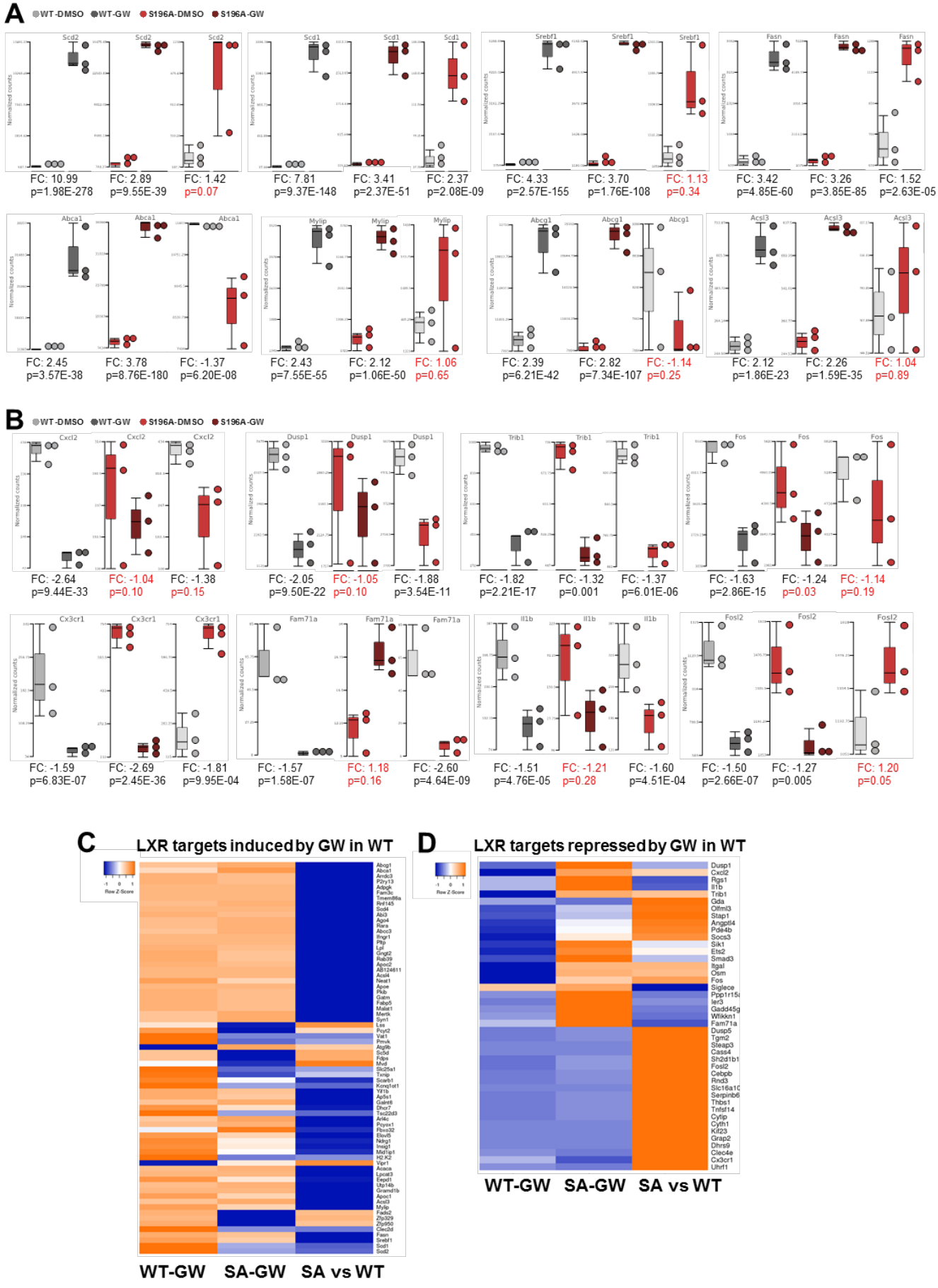

(**A, B**) Combined dot and and box plots depicting normalised RNAseq gene counts showing response to ligand in $WT^{Ldlr\text{-}KO}$ (WT) and M-$S196A^{Ldlr\text{-}KO}$ (S196A) macrophages from WD-fed animals for the top up **(A)** and down **(B)** regulated genes in WT cells. Comparison between DMSO-treated levels between genotypes is also shown. n=3 per genotype or treatment. Fold changes and p values adjusted after FDR 0.05 are shown. Highlighted in red are comparisons that are not statistically significant. (**C, D**) Clustered heatmaps depicting fold changes of all genes significantly (**C**) induced or (**D**) reduced by GW in WT cells (>1.3 fold change, $p< 0.01$), compared to response to GW in S196A, and the expression in S196A vs WT macrophages.

Supplementary Figure 9

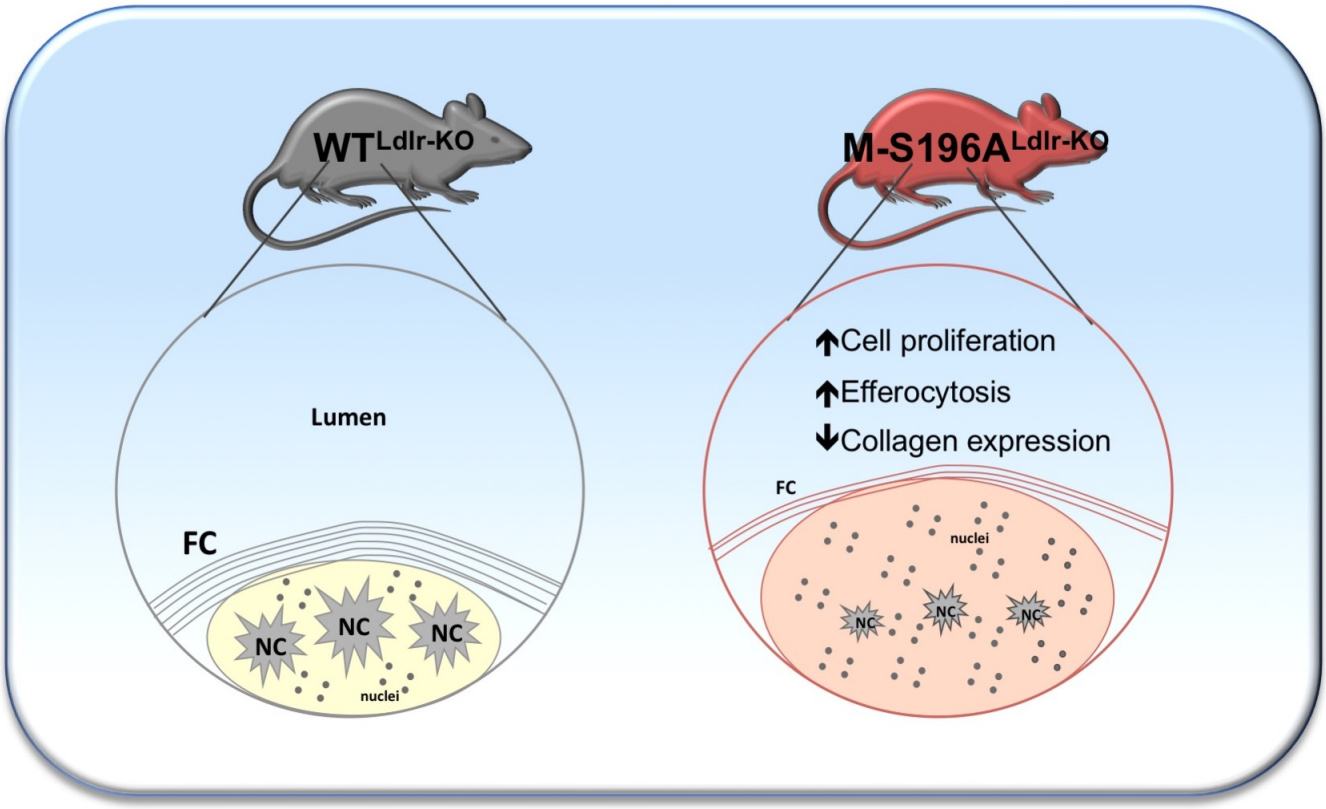

Expression of LXRα-S196A in cells of the myeloid lineage (M-S196A) during the progression of atherosclerosis results in increased atherosclerotic plaque burden associated with plaques that display a distinctive phenotypic profile with (1) increased proliferation of lesion-resident cells, (2) increased apoptotic cell removal by macrophages leading to smaller necrotic cores (NC) and (3) reduced collagen levels and thinner fibrous caps (FC).

Supplementary Figure 10

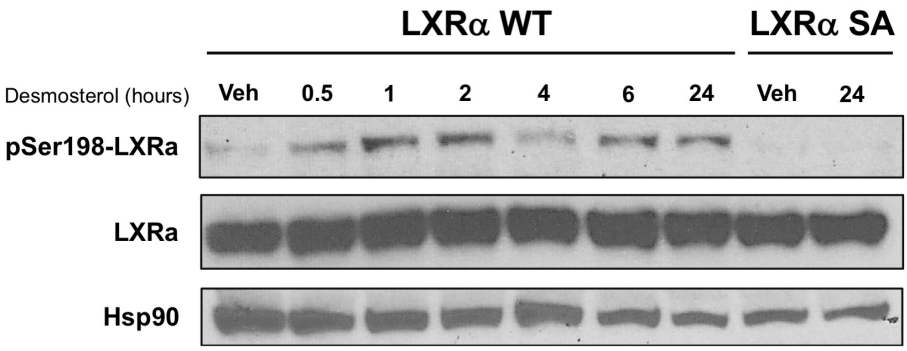

RAW 264.7 cells stably expressing the human LXRα (RAW-hLXRα) or the S198A phospho-mutant (RAW-S198A, equivalent to S196 in the mouse sequence) were incubated with 10 μM Desmosterol or vehicle (Veh) for the indicated periods of time. Nuclear extracts were extracted and phospho-LXRα, total LXRα and Hsp90 were detected by immunoblotting. Shown is a representative experiment of two.

Table S1: Overrepresentation Enrichment Analysis of Reactome Pathways enriched in genes *induced* in S196A

Geneset ID	Name	Gene n	FDR	P
R-MMU-1640170	Cell Cycle	69	0	0
R-MMU-69278	Cell Cycle, Mitotic	57	0	0
R-MMU-68877	Mitotic Prometaphase	23	7.94E-11	1.93E-13
R-MMU-2500257	Resolution of Sister Chromatid Cohesion	22	1.27E-10	4.11E-13
R-MMU-69620	Cell Cycle Checkpoints	29	1.61E-09	6.55E-12
R-MMU-68886	M Phase	30	1.11E-07	5.39E-10
R-MMU-69481	G2/M Checkpoints	22	1.65E-06	9.38E-09
R-MMU-453279	Mitotic G1-G1/S phases	21	1.75E-06	1.14E-08
R-MMU-5663220	RHO GTPases Activate Formins	18	2.72E-06	1.99E-08
R-MMU-68882	Mitotic Anaphase	22	5.39E-06	4.38E-08

Table S2: Overrepresentation Enrichment Analysis of Reactome Pathways enriched in genes *reduced* in S196A

Geneset ID	Name	Gene n	FDR	P
R-MMU-168256	Immune System	43	3.29E-06	2.67E-09
R-MMU-166663	Initial triggering of complement	6	5.81E-06	9.44E-09
R-MMU-3000178	ECM proteoglycans	7	2.49E-05	6.06E-08
R-MMU-166658	Complement cascade	7	3.36E-05	1.09E-07
R-MMU-2022090	Assembly of collagen fibrils	6	7.77E-04	3.16E-06
R-MMU-8948216	Collagen chain trimerization	6	7.84E-04	3.93E-06
R-MMU-1442490	Collagen degradation	7	7.84E-04	4.46E-06
R-MMU-168249	Innate Immune System	29	1.03E-03	6.72E-06
R-MMU-216083	Integrin cell surface interactions	7	1.10E-03	8.03E-06

Table S3: Overrepresentation Enrichment Analysis of Reactome Pathways enriched in genes *induced* in S196A upon GW-activation

Geneset ID	Name	Gene n	FDR	P
R-MMU-1640170	Cell Cycle	35	2.38E-03	1.9E-06
R-MMU-69278	Cell Cycle, Mitotic	29	2.65E-03	4.3E-06
R-MMU-109582	Hemostasis	30	6.36E-03	1.6E-05
R-MMU-2980767	Activation of NIMA Kinases NEK9, NEK6, NEK7	4	6.36E-03	2.1E-05
R-MMU-1538133	G0 and Early G1	6	1.47E-02	6.0E-05
R-MMU-983189	Kinesins	5	2.31E-02	1.1E-04

Table S4: Overrepresentation Enrichment Analysis of Reactome Pathways enriched in genes *reduced* in S196A upon GW-activation

Geneset ID	Name	Gene n	FDR	P
R-MMU-3000178	ECM proteoglycans	6	3.43E-04	6.22E-07
R-MMU-166658	Complement cascade	6	3.43E-04	1.02E-06
R-MMU-2022090	Assembly of collagen fibrils and other multimeric structures	6	3.43E-04	1.28E-06
R-MMU-168256	Immune System	34	3.43E-04	1.39E-06
R-MMU-198933	Immunoregulatory interactions between a Lymphoid and a non-Lymphoid cell	7	2.86E-03	1.60E-05
R-MMU-1474244	Extracellular matrix organization	11	2.86E-03	1.70E-05
R-MMU-216083	Integrin cell surface interactions	6	3.92E-03	3.82E-05
R-MMU-168249	Innate Immune System	24	6.63E-03	8.08E-05
R-MMU-1474228	Degradation of the extracellular matrix	7	7.48E-03	9.72E-05
R-MMU-418594	G alpha (i) signalling events	8	4.59E-02	6.71E-04

Table S5: RT-qPCR primers

Gene	Forward (5' to 3')	Reverse (5' to 3')
Cyclophilin	GGCCGATGACGAGCCC	TGTCTTTGGAACTTTGTCTGCAA
Abca1	GGACATGCACAAGGTCCTGA	CAGAAAATCCTGGAGCTTCAAA
Abcg1	CCTTCCTCAGCATCATGCG	CCGATCCCAATGTGCGA
Srebf1	CAGGAGGACATC TTGCTGCTTC	TTGGGAGGCTGGTTTTGACC
Apoe	CTGACAGGATGCCTAGCCG	CGCAGGTAATCCCAGAGC
Ccr2	GCCATACCTGTAAATGCCATGC	CCAATGCCCTCTTCTGGTCT
Gpr132	TGGCTTGGGTCATTTTAAGC	TCATGGTGGCTCCTATGTGA
Mfge8	GCCTCCCGTTGTTCTACACA	AGACGAGGCGGAAATCTGT
Mertk	GAGCCATCGAGCTTACCTTG	AACTTTGCCGAGAACCAGAA
Gas6	CCGGCTCTGTGACAAAGATG	TTCCTGGTTTGTTGTGGCAG
Foxm1	GAGGTGATCACGGAGACGTT	CTCCTGTCTTTGCCTTGGAG
Ccna2	CTGTCTCTTTACCCGGAGCA	TGTGGTGATTCAAAACTGCCA
Cenpf	GCTTGAAGGACAGCTGGAGA	TCCGCTTTCAACCTTCTGCT
Top2a	GAACATATACTGCTCCGCCC	TTGCTGGGTCACTAACTCCA
Ccnb2	GGCGAAGAAACCTCAGAACA	TCGGCTGCTTGTTGACATTT
Plk1	ATTCCCAAGCACATCAACCC	GGGGTCTGTCTGAAGCATCT
Ccnb1	TGGACTACGACATGGTGCAT	GATGTGCTGCAGAGTTGGTG
Birc5	TGGACAGACAGAGAGCCAAG	CTGCTCAATTGACTGACGGG

Table S6: ChIP-qPCR primers

Gene	Forward (5' to 3')	Reverse (5' to 3')
Abca1	TGAGCTACCCACCCTATGAACA	CCCCTGAACCCAAGGAAGTG
Srebp1c	TCAGCGAGGCGGCTTTGGAG	CATGTCTTCGATGTCGGTCAG
TULP3	AGATGCTCCACCATACCACA	GCACCCCACCCCAAATAAAG
FoxM1 P1	CCCTGCCTCCTGTCTCATAG	AGAAGGGAGAGCTGCTTTGA
FoxM1 LXRE	GAATCTAGGTGAGGGGCTGG	GATGACTGTGAGCTGCCATG
FoxM1 P2	CCCATCGTCTCTCATCCCTC	TGCCTGCCATTGTGTACTAGA
Top2a P2	CCTGAAGGGGAGCTGATTGT	CCTCAAACCTCAGAGCTCCT
Top2a LXRE2	CGGGAAGGTCAGAAGAAGTC	TGTCCTCACCCATACAGAAGAC
Cenpf LXRE2	TGCAGCTCTCTATACCAAATTCC	ATTTTGTGCCTTTAAACTTCCCA